POLITECNICO DI MILANO
SCUOLA DI INGEGNERIA INDUSTRIALE E DELL'INFORMAZIONE
Corso di Laurea Magistrale in Ingegneria delle Telecomunicazioni

Discrete-multitone modulation for short distance 100 Gbit/s optical links

Relatore: Prof. Maurizio MAGARINI
Correlatore: Dr.-Ing. Sebastian RANDEL

Tesi di laurea di:
Dario PILORI
Matr. 796201

Anno Accademico 2014 - 2015

If I have seen further, it is by standing on the shoulders of giants.

Sir Isaac Newton, 1676

To everyone who helped me

Contents

List of acronyms

ABC Automatic Bias Controller

ADC Analog-to-Digital Converter

ADSL Asymmetric Digital Subscriber Line

ASE Amplified Spontaneous Emission

ASIC Application Specific Integrated Circuit

AWGN Additive White Gaussian Noise

BER Bit Error Rate

BPSK Binary Phase-Shift Keying

CD Chromatic Dispersion

CDN Content Delivery Network

CSPR Carrier-to-Signal Power Ratio

CW Continuous Wave

DAC Digital-to-Analog Converter

DC Direct Current

DFE Decision Feedback Equalization

DFT Discrete Fourier Transform

DML Directly Modulated Laser

DMT Discrete Multitone

DSB Dual SideBand

DSP Digital Signal Processing

DTFT Discrete Time Fourier Transform

ECL External Cavity Laser

ECOC European Conference on Optical Communications

EDFA Erbium Doped Fiber Amplifier

EOM Electro/Optical Modulator

FDE Frequency Domain Equalizer

FEC Forward Error Correction

FFT Fast Fourier Transform

I In-Phase

IBI Interblock Interference

IDFT Inverse DFT

IFFT Inverse FFT

ISI Intersymbol Interference

LPF Lowpass Filter

ML Maximum Likelihood

MMSE Minimum Mean Square Error

MZM Mach-Zehnder Modulator

NRZ Non-Return-to-Zero

OFC Optical Fiber Conference

OFDM Orthogonal Frequency Division Multiplexing

OOK On-Off Keying

OSA Optical Spectrum Analyzer

PAM Pulse Amplitude Modulation

PAPR Peak-to-Average Power Ratio

PBS Polarization Beam Splitter

PDM Polarization Division Multiplexing

PM Polarization Maintaining

POF Plastic Optical Fiber

PSD Power Spectral Density

Q Quadrature

QAM Quadrature Amplitude Modulation

QPSK Quadrature Phase-Shift Keying

RF Radio Frequency

SBS Stimulated Brillouin Scattering

SNR Signal-to-Noise Ratio

SOA Semiconductor Optical Amplifier

SSB Single Side-Band

SSBI Signal-Signal Beating Interference

SSMF Standard Single-Mode optical Fiber

TIA Transimpedance Amplifier

VCSEL Vertical-cavity surface-emitting laser

VOA Variable Optical Attenuator

WDM Wavelength Division Multiplexing

XGM Cross Gain Modulation

XPM Cross Phase Modulation

ZF Zero-Forcing

ZWP Zero Water Peak

List of Figures

List of Tables

Abstract

The commercially available 100 Gbit/s optical channel employs coherent modulation and demodulation allowing transmission over long distances, up to thousands of kilometers, but for short distances the cost of a coherent receiver can be overkill. In literature there are several techniques, based on advanced different digital modulation schemes, that reduce the complexity of the transmitter or the receiver, allowing a more cost-effective solution. The contribution of this work is the design and implementation of a communication system employing Discrete Multitone (DMT) modulation with bit and power loading, transmitted using an externally modulated laser in C-band, optically amplified, and received with a single photodiode (direct detection). After the design of the system followed by numerical simulations, it has been experimentally tested both in back-to-back and over several spans of Standard Single-Mode optical Fibers (SSMFs), up to 80 km. We studied and adopted Single Side-Band (SSB) at the transmitter to increase spectral efficiency and reduce the effects of Chromatic Dispersion (CD).

This work is organized as follows. After the introduction, in chapter 2 we present the main concepts of optical communications. Chapter 3 presents the theory of multi-channel modulation (such as DMT), comparing it with single-channel techniques. Chapter 4 shows channel capacity for multi-channel modulation scheme and the Levin-Campello bit and power loading algorithm.

After reviewing the state-of-the-art, in chapter 5 is presented the system design, along with the algorithms we developed, and the experimental setup; the results are showed in chapter 6. The results we obtained are very promising since we measured a pre-Forward Error Correction (FEC) Bit Error Rate (BER) below the standard hard-decision FEC threshold. Chapter 7 presents the conclusions of this work.

Sommario

Il canale ottico a 100 Gbit/s comunemente utilizzato nei sistemi commerciali impiega una modulazione e demodulazione coerente, e ciò permette di trasmettere a lunghe distanze, dell'ordine di migliaia di chilometri, ma per trasmissioni su brevi distanze il costo di un sistema di trasmissione coerente può essere eccessivo. In letteratura sono presentate varie soluzioni, basate su diversi schemi di modulazione digitali che riducono la complessità del trasmettitore o del ricevitore, e questo permette di ridurre il costo. Il contributo di questo lavoro è lo sviluppo e l'implementazione di un sistema di comunicazione ottico basato sulla modulazione Discrete Multitone (DMT), trasmesso con un laser modulato esternamente nella banda C, amplificato con Erbium Doped Fiber Amplifier (EDFA) e Semiconductor Optical Amplifier (SOA), e ricevuto con un singolo fotodiodo (rilevazione diretta). Dopo la progettazione del sistema e la sua simulazione numerica, abbiamo costruito un apparato sperimentale in cui abbiamo trasmesso il segnale a 100 Gbit/s sia in condizione *back-to-back* (ossia trasmettitore collegato direttamente al ricevitore con pochi metri di fibra), che lungo diverse distanze di fibra ottica standard monomodale (SSMF), fino a 80 km. Abbiamo adottato una trasmissione a banda laterale singola (SSB) per aumentare l'efficienza spettrale e ridurre l'impatto della dispersione cromatica (CD), che, non compensata, è deleteria per distanze superiori a qualche chilometro.

Questa tesi è organizzata come segue. Dopo l'introduzione, nel capitolo 2 vengono presentati i concetti fondamentali dei sistemi di comunicazione ottici, entrando nel dettaglio sui principi utilizzati per questa tesi, come il modulatore Mach-Zehnder (MZM) in niobato di litio ($LiNbO_3$), rilevazione diretta di un segnale modulato in ampiezza, dispersione cromatica e compensazione usando un segnale SSB. Nel capitolo 3 viene presentata la teoria dei sistemi di trasmissione multicanale, comparandoli con i sistemi a singolo canale, e spiegando nel dettaglio i sistemi Orthogonal Frequency Division Multiplexing (OFDM) e DMT. Nel capitolo 4 viene illustrata la capacità del canale DMT, mostrando l'importante risultato che un sistema multicanale con allocazione ottimale di potenza tra le sottoportanti può ottenere la capacità di un sistema a singolo canale con equalizzatore Minimum Mean Square Error (MMSE)-Decision Feedback Equalization (DFE) a lunghezza infinita. A partire da questi risultati viene mostrato l'algoritmo Levin-Campello per l'allocazione di bit e potenza sulle varie sottoportanti con una bassa complessità computazionale.

Dopo la revisione dello stato dell'arte, nei capitoli successivi viene presentato il contributo di questa tesi, dal dimensionamento del sistema ai risultati sperimentali. Il capitolo

5 presenta il dimensionamento dei vari sottosistemi, illustrando gli algoritmi di Digital Signal Processing (DSP) usati nel trasmettitore e ricevitore e la loro implementazione, spiengando infine l'apparato sperimentale. Nel capitolo 6 sono illustrati i risultati ottenuti con l'apparato sperimentale, dove, dopo una calibrazione iniziale del sistema per trovare i parametri ottimali, vengono mostrate le curve di Bit Error Rate (BER) sia in back-to-back con l'aggiunta di rumore Amplified Spontaneous Emission (ASE), che dopo 20, 60 e 80 km di SSMF. I risultati sono molto promettenti dato che abbiamo misurato a 80 km un tasso di errore (BER) non codificato sotto la soglia di 3.8×10^{-3} della codifica di canale scelta. Nel capitolo 7 vengono illustrate le conclusioni con le problematiche restanti per sviluppare un prodotto commerciale.

Chapter 1

Introduction

Current transport networks are almost entirely built with optical fiber.

Research in communication over optical fiber started in the 1960s with the construction of the first laser [22] and optical fiber itself [17]. In the 1970s fiber technology was further developed making actually possible to transmit information over optical fiber, and in the 1980s started the first commercial deployments of optical fiber. Research was led by the fact that the electrical transmission technologies, namely coaxial cables and microwave links, were inadequate even at that period for transmission of high bitrates over long distances.

Current high-speed optical transport systems are based on the 100 Gbit/s channel [41], which employs Polarization Division Multiplexing (PDM)-Quadrature Phase-Shift Keying (QPSK) coherent modulation and demodulation techniques for a line (gross) rate of 112 Gbit/s; the coherent receiver will be explained in detail in section 2.2.2. The 100G technology, initially developed in mid 2000s [40], started its commercial deployments in 2010s [39], and now is a mature and widely deployed technology. Systems with higher speed are already commercially available and tested in field trials [27], and research is going even further with single channel speed [32].

The coherent 100G channel has been proven flexible and efficient, but for short and medium haul systems (up to 80 km), employed in metro networks, the standard 100G channel can be overkill due to its high costs and complexity. A recent study by Cisco [11] showed that in the next years metro networks will become more important due to the use of Content Delivery Networks (CDNs) for video streaming, therefore there is a growing research interest in these networks.

Several novel techniques have been proposed to tackle this problem [34], based on advanced Digital Signal Processing (DSP) made possible due to the availability of fast Analog-to-Digital Converters (ADCs) and Digital-to-Analog Converters (DACs); one of the most promising techniques is Discrete Multitone (DMT). DMT has been developed in the 1990s [7] for the use in Asymmetric Digital Subscriber Line (ADSL) systems (leading to the ITU-T Recommendation G.992.1 [12]), was then proposed in the end of 2000s for the use in Plastic Optical Fiber (POF) [18, 19], and during the last years its use was proposed, initially by Fujitsu for 100G Ethernet [37], for medium reach optical transport

systems (up to 80 km), with several experiments made by different companies [6, 25, 43].

Another novel application for DMT modulation are short-reach optical interconnects, such as data-center communications, where, paired with cost-effective Directly Modulated Lasers (DMLs) like Vertical-cavity surface-emitting lasers (VCSELs), allow 100G communications at an even smaller cost. Another work that we performed, using similar software and experimental setup as the work done in this thesis, proved reliable transmission up to 4 km of Standard Single-Mode optical Fiber (SSMF) [42].

Project goals

The final goal of this work is the development of a DMT-based medium reach cost-effective communication system, suitable for 100G communications up to 80 km.

A special focus have been put in the complexity of the DSP algorithms for a future implementation in an Application Specific Integrated Circuit (ASIC), and we put the following constraints in order to reduce the cost and the complexity of the system:

- The communication is strictly unidirectional, without any feedback from the receiver to the transmitter;
- The receiver is based on a single photodetector;
- Transmission is performed over SSMF (ITU-T Recommendation G.652 [14], Table B) over C-band (1550 nm).

Outline

This work is organized as follows. In chapter 2 we present the main concepts of optical communications adopted for this work. We start discussing on the different techniques used for modulation and detection of an optical signal, leading to the *self-coherent* solution as a trade-off between performance and complexity. We then present the features of C-band, with its advantages, such as low loss and amplification with Erbium Doped Fiber Amplifiers (EDFAs), and the main disadvantage of Chromatic Dispersion (CD). We then present Single Side-Band (SSB) as a solution to compensate for CD and increase spectral efficiency.

Then, in chapter 3, we present the theory digital communication focusing on the techniques which can be used in the optical channel presented in chapter 2. We then explain the differences between single-channel and multi-channel modulation, describing in detail multi-channel schemes, such as Orthogonal Frequency Division Multiplexing (OFDM) and DMT.

One of the main advantages of multi-channel modulation is the possibility to use different power and modulation schemes for each subchannel, and this can be exploited to increase the overall throughput. To do this, in chapter 4 we evaluate channel capacity for multi-channel modulation, showing the important result that, with an optimal allocation of bits and power, we can achieve the capacity of single-channel system followed by an infinite-length Minimum Mean Square Error (MMSE)-Decision Feedback Equalization

(DFE) equalizer, which is difficult to implement in a receiver for optical communications. After that, we describe the allocation algorithms, leading to the Levin-Campello scheme, which is the scheme we adopted in this work.

In chapter 5 we start presenting the contribution of this thesis, starting from the detailed implementation of the DSP algorithms for DMT modulation and demodulation. We then provide some calculations that we derived to solve some practical issues we encountered in the system design, such as the high Peak-to-Average Power Ratio (PAPR), the delay between the In-Phase (I) and Quadrature (Q) components at the transmitter and the Signal-Signal Beating Interference (SSBI), which is one of the main impairments of self-coherent systems. After this, we show some models we developed to measure and control the Carrier-to-Signal Power Ratio (CSPR), which is one of the most important parameters of our transmitter, and we provide a model to predict the impact of transmitter imbalances on a SSB system. At the end, we show the experimental setup we built to test the system we developed.

The experimental results are shown in chapter 6. At the beginning we calibrate the main parameters of the system (CSPR, transmit and receive powers) in optical back-to-back, and we produce a Bit Error Rate (BER) curve with Amplified Spontaneous Emission (ASE) noise loading with the aid of a Variable Optical Attenuator (VOA). Then we transmit over several spools of SSMF, up to 80 km and, after another calibration, we provide the BER curves with respect to the launch power. We anticipate that the results are very promising, showing a BER under the Forward Error Correction (FEC) threshold at 80 km with reasonable transmitter and receiver parameters, and this means that, with further investigation, a commercial system can be built. The conclusions are detailed in chapter 7.

Publications

The main part of this work has been accepted for oral presentation at European Conference on Optical Communications (ECOC) 2015 [31]. The presentation focuses on the SSBI compensation algorithm, the system design and the experimental results.

Additionally, a related work, where we transmitted 100 Gbit/s DMT modulation with a directly modulated VCSEL over data center distances (up to 4 km), has been presented at Optical Fiber Conference (OFC) 2015 [42].

Chapter 2

Optical communications

In this chapter we will introduce optical fiber as a transmission media, focusing on the different receiver and transmitter structures and their characteristics, and from them we will present the self-coherent system as a compromise between coherent and non-coherent communications. After these, we will explain the issue of chromatic dispersion and we will present the method used in this work for compensating it. The main reference used in this chapter is [1].

2.1 Introduction

A generic scheme of an optical communication system is shown in Figure 2.1.

The goal is reliably transmit bits from the source to the sink. The source sends bits to the electrical transmitter, which maps the bits into an analog waveform $x(t)$. Usually the electrical transmitter is digital, *i.e.* all the processing is done digitally, and as a last step a DAC generates the analog waveform.

The analog waveform is then used to modulate an optical carrier, *e.g.* light coming from a laser, using a device called Electro/Optical Modulator (EOM); we use f_0 to indicate the carrier frequency, or equivalently $\lambda_0 = c/f_0$ in terms of wavelength. The modulated light is then sent into an optical transmission system, which consists in various spans of optical fiber with some optical amplifiers to recover signal amplitude.

The light is then received by an optical receiver, that transform the incident optical

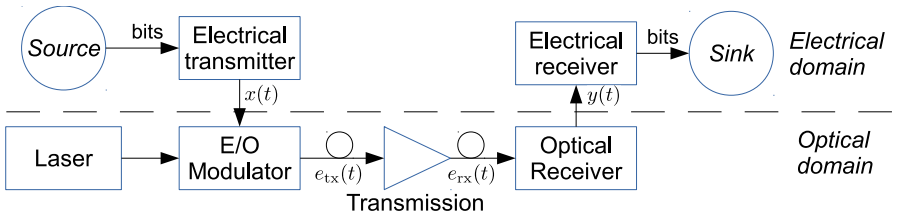

Figure 2.1: Generic optical communications system (from [1, ch.1])

field into an electrical analog waveform $y(t)$, which is sent to the electrical receiver that tries to recover the original transmitted bits and sends them to the sink. Like the electrical transmitter, the electrical receiver is digital as well, so that its first component is an ADC and all the processing is done in the digital domain.

2.2 Optical receiver

In optical communications, the choice of the receiver limits the capabilities of the transmitter, therefore it is explained before the transmitter.

2.2.1 Photodiode

An optical signal is a passband signal, so its baseband representation is a complex signal (baseband signals are described in detail in appendix A.2). The main device to transform an optical field into an electrical signal that can be detected with an ADC, the *photodiode*, is sensible only the *intensity* (*i.e.* the squared modulus) of the electric field [1, ch.3].

A PiN photodiode, for instance, works thanks to a junction of a p-doped semiconductor, an intrinsic material and a n-doped semiconductor. In this work we will always assume that the photodiode is ideal, *i.e.* its output current is proportional to the intensity of the incident electric field in both polarizations

$$i(t) \propto |e(t)|^2 \tag{2.1}$$

This is a big limitation, because allows only to receive amplitude modulated signals, with a waste of spectral efficiency and power.

2.2.2 Coherent receiver

In order to detect the real and the imaginary part of the incident optical field we have to add a carrier to the received signal immediately before the photodiode. We assume that the carrier is a Continuous Wave (CW) light source with amplitude c and phase 0. The received signal, in complex baseband, therefore is

$$y(t) = |e(t) + c|^2 = |e(t)|^2 + c^2 + 2c\Re\{e(t)\} \tag{2.2}$$

The presence of the carrier unlocks the access to the real part of the electric field, with two unwanted terms. While c^2 is a DC tone and can be removed using a DC block, $|e(t)|^2$ is a nonlinear distortion of the incident electric field whose removal is not trivial. To remove these terms, we add another arm in which a phase shift of π is applied to the carrier and we connect it to a second photodiode, leading to

$$\begin{cases} y_1(t) = |e(t) + c|^2 = |e(t)|^2 + c^2 + 2c\Re\{e(t)\} \\ y_2(t) = |e(t) - c|^2 = |e(t)|^2 + c^2 - 2c\Re\{e(t)\} \end{cases}$$

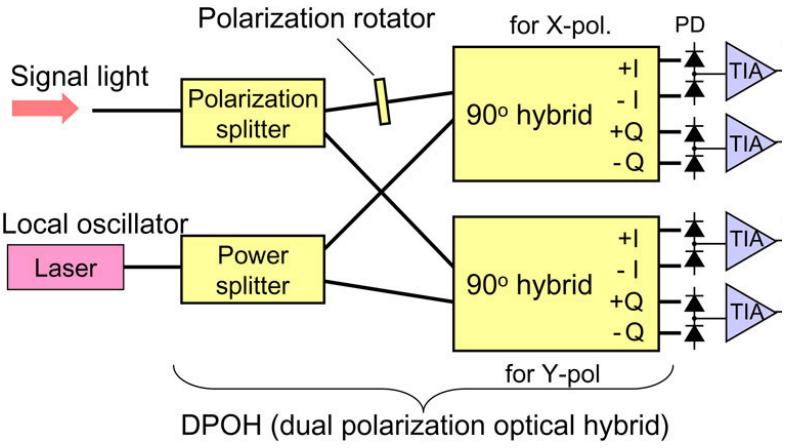

Figure 2.2: Coherent receiver scheme

Considering the difference $y_1(t) - y_2(t)$ we finally get

$$y_1(t) - y_2(t) = 4c\Re\{e(t)\}$$

The imaginary part can be obtained with a $\pi/2$ phase shift to the carrier in the same way as the real part

$$\begin{cases} y_3(t) = |e(t) - jc|^2 = |e(t)|^2 + c^2 + 2c\Im\{e(t)\} \\ y_4(t) = |e(t) + jc|^2 = |e(t)|^2 + c^2 - 2c\Im\{e(t)\} \end{cases}$$

and

$$y_3(t) - y_4(t) = 4c\Im\{e(t)\}$$

For this derivation we assumed an unpolarized input optical field; in case we want to detect both polarizations we have to split using a Polarization Beam Splitter (PBS) the signal in two orthogonal polarizations and do the same for the carrier, leading to the *coherent receiver* [1, ch.10] , shown in Figure 2.2. The receiver with only one photodiode described in section 2.2.1 is called *non-coherent receiver*.

It is important to note that in order for the coherent receiver to work properly, the phase (so the length) of the arms must be accurately controlled, so it is usually performed in an integrated device called 90° hybrid. The two photodiodes and the difference operation are done in another integrated device called *balanced* photodetector.

2.3 Optical transmitter

There are two main ways to modulate an optical carrier:

- Direct modulation
- External modulation

With direct modulation we change the properties (*e.g.* the input current) of the CW source to modulate the optical field, while with external modulation a device called *optical modulator* is used to modulate the optical field.

The main device used for the external modulation is the Mach-Zehnder Modulator (MZM), which is the device used in this work.

Mach-Zehnder Modulator

The MZM is an integrated optical device that consists in a Mach-Zehnder interferometer with two electrodes that, exploiting Pockels effect, create a phase difference between the two arms proportional to an input voltage $V(t)$ [2]. These devices can be made with different materials, such as silicon (Si), indium phosphide (InP) or lithium niobate ($LiNbO_3$). In this work we used a lithium niobate modulator, since they have a large modulating bandwidth with a small driving voltage, with the main drawback of the size[1], which makes difficult an integration with the transmitter.

The phase difference between the two arms can be modeled as

$$\Delta\phi(t) = \pi\frac{V(t)}{V_\pi}$$

where V_π is a construction parameter of the modulator and represents the voltage that achieves a π phase shift between the two arms.

The output optical field, assuming a CW input, is therefore

$$e_{\text{out}}(t) \propto \frac{1}{2}\left(e^{j\pi\frac{V(t)}{2V_\pi}} + e^{-j\pi\frac{V(t)}{2V_\pi}}\right) = \cos\left(\pi\frac{V(t)}{2V_\pi}\right) \tag{2.3}$$

which means that we can modulate the amplitude of the real part of the electric field; this response is shown in Figure 2.3.

The main problem is that this transfer function is not linear, so in order to use it we have to use a modulating voltage $V_{\text{rf}}(t) \ll V_\pi$ and add a DC bias V_{b} to set a working point where we can linearize the function. Most of the modulators have two separated electrodes, each with its own V_π, one for the RF voltage input $V_\pi^{(\text{rf})}$ and one for the bias input $V_\pi^{(\text{dc})}$, leading to

$$e_{\text{out}}(t) \propto \cos\left(\frac{\pi}{2V_\pi^{(\text{rf})}}V_{\text{rf}}(t) + \frac{\pi}{2V_\pi^{(\text{dc})}}V_{\text{b}}\right)$$

There are two main bias points:

- The *null* point $V_{\text{b}} = -V_\pi^{(\text{dc})}$ is the point where the amplitude response is maximally linear.

[1] The modulator we used is $79.4 \times 13.5 \times 7$ mm, and they can be as long as 10 cm

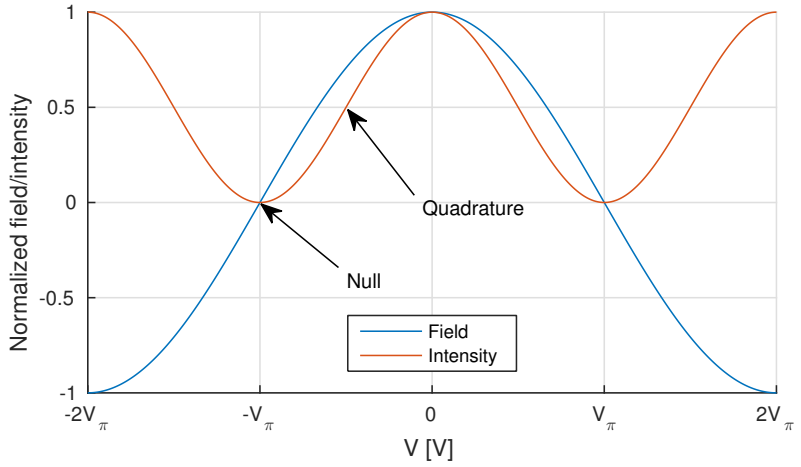

Figure 2.3: Mach-Zehnder Modulator response

- The *quadrature* point $V_{\mathrm{b}} = -V_{\pi}^{(\mathrm{dc})}/2$ is the point where the intensity response

$$I_{\mathrm{out}}(t) = |e_{\mathrm{out}}(t)|^2 \propto \frac{1}{2} + \frac{1}{2}\cos\left(\frac{\pi}{V_{\pi}^{(\mathrm{rf})}}V_{\mathrm{rf}}(t) + \frac{\pi}{V_{\pi}^{(\mathrm{dc})}}V_{\mathrm{b}}\right)$$

  is maximally linear.

The choice of the bias point depends on the adopted modulation scheme, which mainly depends on the receiver capabilities.

If field modulation is adopted, then the modulator is biased at the null, while if intensity modulation is adopted then the modulator is biased at the quadrature.

Dual-nested MZM

The MZM described with equation (2.3) allows us to modulate only the real part of the electric field. To modulate the whole optical field we add another modulator combined to a $\pi/2$ phase shift which modulates the imaginary part of the optical field. This device is called *dual-nested* MZM.

Its structure is shown in Figure 2.4. A third bias voltage V_{b3} is responsible of the $\pi/2$ phase shift, while the two arms are controlled independently. To control both polarizations, two dual-nested MZMs are put in parallel, preceded and followed by a PBS.

In the following sections we will use the term MZM to indicate a single-polarization dual-nested Mach-Zehnder modulator.

2.4 Self-coherent systems

The choice of a receiver is a critical parameter in the design of an optical communication system. A coherent receiver allows to use modulation formats with very high spectral

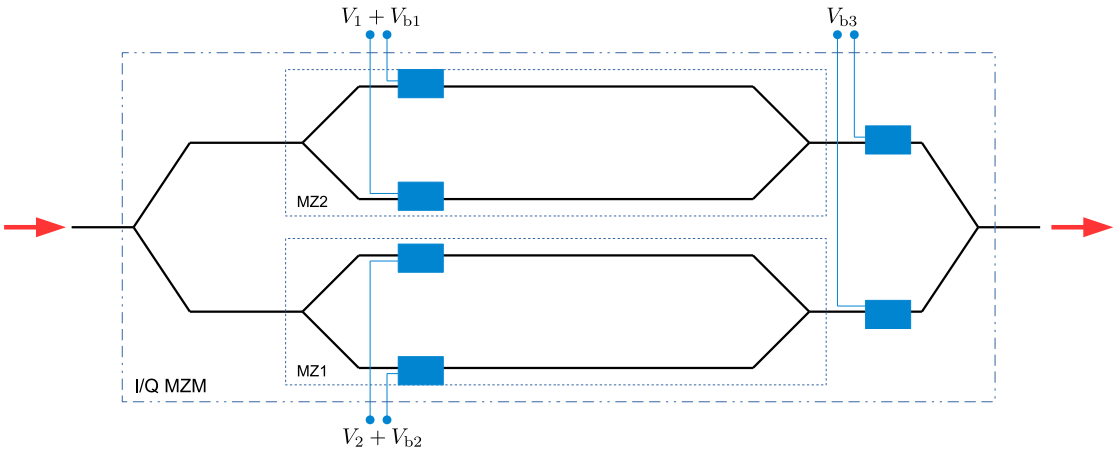

Figure 2.4: Dual-nested Mach-Zehnder modulator

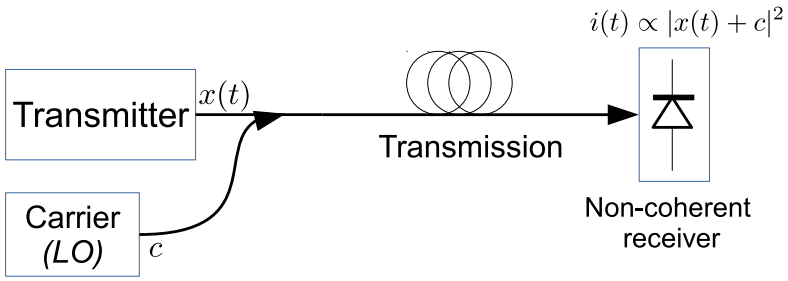

Figure 2.5: Self-coherent scheme

efficiency, but has high costs, since it needs not only the components inside the receiver, but also 4 ADCs and some DSP algorithms to perform a carrier recovery to compensate the difference between the transmit laser and the local oscillator.

On the other end, a single photodiode is very simple and cost-effective, but the traditional choice of intensity modulation schemes has very low spectral efficiency and cannot achieve high bit-rates.

It is then important to find a third solution, which lays in between these two, and this solution is *self-coherent*.

2.4.1 Structure

The scheme of a self-coherent system is shown in Figure 2.5. The receiver is a regular non-coherent receiver, but a carrier is added to the signal *at the transmitter*.

The solution is the same as equation (2.2)

$$y(t) = |e(t)|^2 = c^2 + \underbrace{|x(t)|^2}_{ss(t)} + 2c\underbrace{\Re\{x(t)\}}_{sc(t)} \tag{2.4}$$

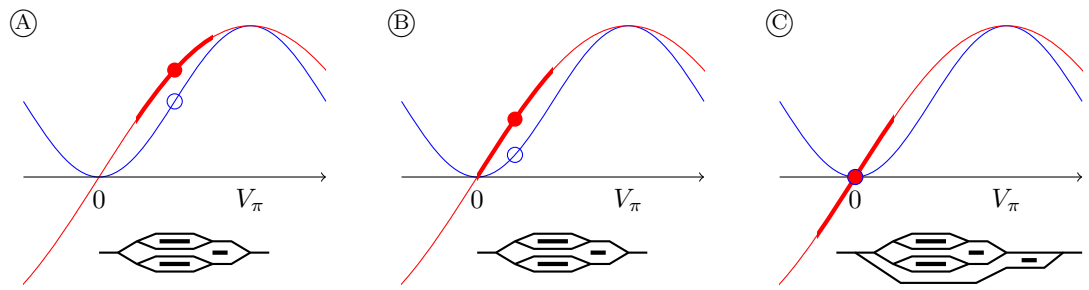

Figure 2.6: Self-coherent transmitter structures

where we call the square term SSBI $ss(t)$ and the real part term *signal-carrier beating* $sc(t)$.

This scheme allows the use of a single photodiode to detect the real part of the signal, with two main disadvantages:

- The signal is corrupted by SSBI, which cannot be removed optically like in the coherent receiver since we cannot separate carrier and signal at the receiver
- We waste transmit power since must be divided between signal and carrier; moreover, a high power concentrated in a single wavelength can increase the impact of fiber nonlinearities

While the first disadvantage can be, at least partially, compensated using DSP, the second one is limiting the range of the self-coherent system to hundreds of kilometers. Since our goal is transmission over 80 km, this disadvantage is not a limitation, while the first one will be discussed in the DSP section.

Obviously since it is able to detect only the real part of the optical field a self-coherent system needs a real modulation scheme (*e.g.* PAM), so we will always assume that the transmitted signal is real in complex baseband. A discussion of the possible real modulation formats will be performed in chapter 3.

2.4.2 Transmitter structures

The generation of a self-coherent signal is not trivial since it requires to add the same carrier used to modulate the signal. There are three different approaches to achieve this, shown in figure 2.6. At the top of the figures the amplitude (red) and the intensity (blue) response of the MZM is shown, the dot is the bias point while the bold line is the signal amplitude range. On the bottom the structure of the MZM is shown.

- In scheme Ⓐ we bias the modulator at the quadrature point and the CSPR is controlled by changing the Radio Frequency (RF) signal amplitude. The main drawback of this scheme is the high modulator nonlinearity and the need of a broadband linear driver amplifier.

- In scheme Ⓑ we bias in a point between the null and the quadrature, and we tune the CSPR by changing the bias point. The modulator nonlinearities are lower but it is difficult to implement an automatic bias control for this point.

- In scheme Ⓒ we bias at the null and the carrier is added from an external path. This scheme has the lowest modulator nonliearities, but requires a modification of the modulator; this scheme also requires a tight control of the phase of the carrier

We tried solutions Ⓑ and Ⓒ; solution Ⓐ was not possible since we did not have suitable driver amplifiers, and its cost would be too high for the project goals.

The practical realization of these two structures and their results will be discussed in chapters 5 and 6.

2.5 Fiber propagation

The linear effects of propagation of an optical field $e_{\text{tx}}(t)$ over d meters of optical fiber can be approximated using the expression

$$E_{\text{rx}}(f) = E_{\text{tx}}(f) \cdot 10^{-\alpha d/20} e^{-j\beta(f)d} \tag{2.5}$$

where α[dB/m] is called *attenuation* factor and represents an amplitude decay of the signal, $\beta(f)$ is a phase variation of the signal that, in general, depends on the signal frequency. It can be expanded using a Taylor series around 0 to get [2]

$$\beta(f) \approx \underbrace{\beta(0)}_{\beta_1} + \underbrace{\frac{\mathrm{d}\beta}{\mathrm{d}f}\bigg|_{f=0}}_{\beta_1} \cdot f + \frac{1}{2}\underbrace{\frac{\mathrm{d}^2\beta}{\mathrm{d}f^2}\bigg|_{f=0}}_{\beta_2} \cdot f^2$$

Let us analyze these three parameters:

- β_0 is a frequency-independent phase shift

- β_1 is a linear phase shift and represents a delay in time; this is linked to the propagation velocity (called *group velocity*) of the signal

$$v_{\text{g}} = \frac{2\pi}{\beta_1}$$

[2] It is important to note that in some references (like [3]) the terms β_1 and β_2 are obtained by taking the derivatives of β with respect to $\omega = 2\pi f$ instead of f; however, the definition of D_λ, which is the main parameter used to quantify chromatic dispersion, has been modified in order to get the same result.

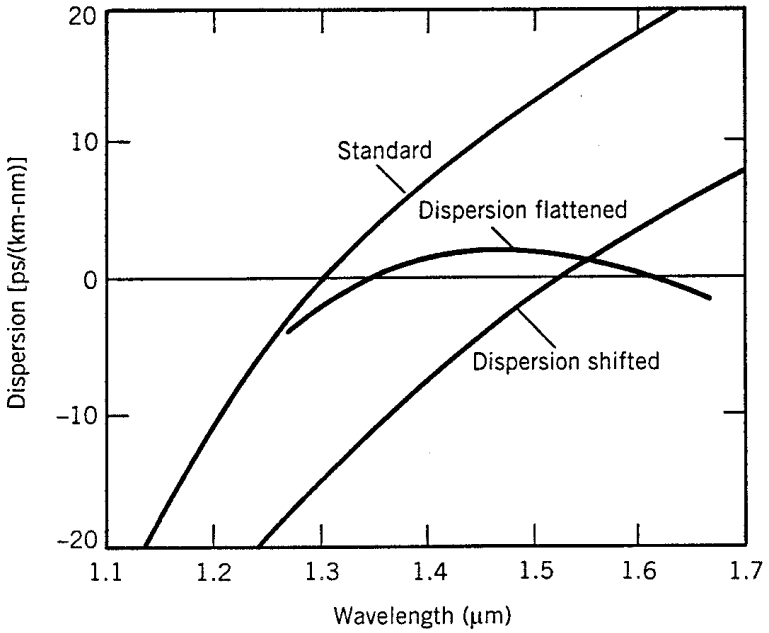

Figure 2.7: Chromatic dispersion in various types of optical fiber (from [1, ch. 2])

- β_2 is a linear change of the group velocity depending on the frequency

While the term β_0 can be easily compensated at the receiver, the term β_2 makes the different frequency components of the transmit signal travel at different velocities and its effect is called *chromatic dispersion.*

2.5.1 Chromatic dispersion

Chromatic dispersion is an effect that creates memory in the channel. An approximate formula gives the broadening of a pulse with bandwidth Δf [1, p. 39]

$$T \approx d\Delta f \frac{\beta_2}{2\pi}$$

In optics, bandwidths are usually expressed as difference between wavelengths $\Delta\lambda$. Using the relation

$$\Delta f \approx -\frac{c}{\lambda_0^2}\Delta\lambda = -\frac{f_0^2}{c}\Delta\lambda$$

where c is the speed of light in vacuum and f_0 the center frequency of the signal, we can create another parameter to measure chromatic dispersion

$$D_\lambda = -\frac{f_0^2}{2\pi c}\beta_2$$

so that

$$T \approx d\,\Delta\lambda\,D_\lambda$$

D_λ is usually expressed in units of ps/(nm · km) ($1\,\text{ps/(nm}\cdot\text{km)} = 1\times10^{-6}\,\text{s/m}^2$), and a plot of its value for different kinds of optical fiber is shown in Figure 2.7. SSMF has zero chromatic dispersion in O-band around 1310 nm, while in C-band its value is approximately 19 ps/(nm · km).

With a coherent receiver, since we have full access to the received electric field, chromatic dispersion can be fully compensated using a linear filter with frequency response $\exp\left(-j\hat{\beta}_2 f^2 d/2\right)$, where $\hat{\beta}_2$ is the estimation of the chromatic dispersion [35]. In a self-coherent system uncompensated chromatic dispersion will irreversibly degrade system performance. To understand this, let us write the signal-carrier beating using a passband signal $e_{\text{pb}}(t)$

$$2\Re\{e_{\text{pb}}(t)e^{-j2\pi f_0 t}\} \xrightarrow{\mathcal{F}} E_{\text{pb}}(f+f_0) + E^*_{\text{pb}}(-f+f_0)$$

Graphically this operation is shown in Figure 2.8, where we neglected the two additional terms at $f = \pm 2f_0$. As we can see, around baseband the negative frequency spectrum and the positive frequency spectrum are summed with different chromatic dispersion phases, and this destructive interference will degrade the performance and irreversibly reduce the SNR.

Going back to complex baseband, the signal-carrier beating of the real optical field $e(t)$ affected by chromatic dispersion (represented by the linear filter $h_{\text{cd}}(t)$) becomes [3]

$$\begin{aligned} sc(t) &= \Re\left\{e(t)\otimes h_{\text{cd}}(t)\right\} \xrightarrow{\mathcal{F}} E(f)e^{-j\beta_2 f^2 d/2} + E^*(-f)e^{j\beta_2 f^2 d/2} = \\ &= 2E(f)\cos\left(\frac{1}{2}\beta_2 f^2 d\right) \end{aligned}$$

where the cosine creates ripples in the spectrum that degrades the performance of the system.

Compensation techniques

There are different strategies used to reduce the impact of chromatic dispersion in non-coherent short-distance links. The best strategy would be transmitting in O-band around the zero of chromatic dispersion, like [6, 43]. The use of dispersion-shifted fiber [13] is not recommended due to high nonlinearities.

Since in our system we are required to use C-band over SSMF, we adopted another solution, which will be explained in detail in section 2.6.

2.5.2 Attenuation

As for any guided transmission method (like coaxial cables), a signal transmitted over optical fiber is, according to (2.5), exponentially attenuated with factor α (dB/km). The attenuation profile of SSMF over different bands is shown in Figure 2.9.

According to the attenuation profile, optical fiber bandwidth is conventionally divided into bands, shown in table 2.1, defined in ITU-T series G supplement 39 [15].

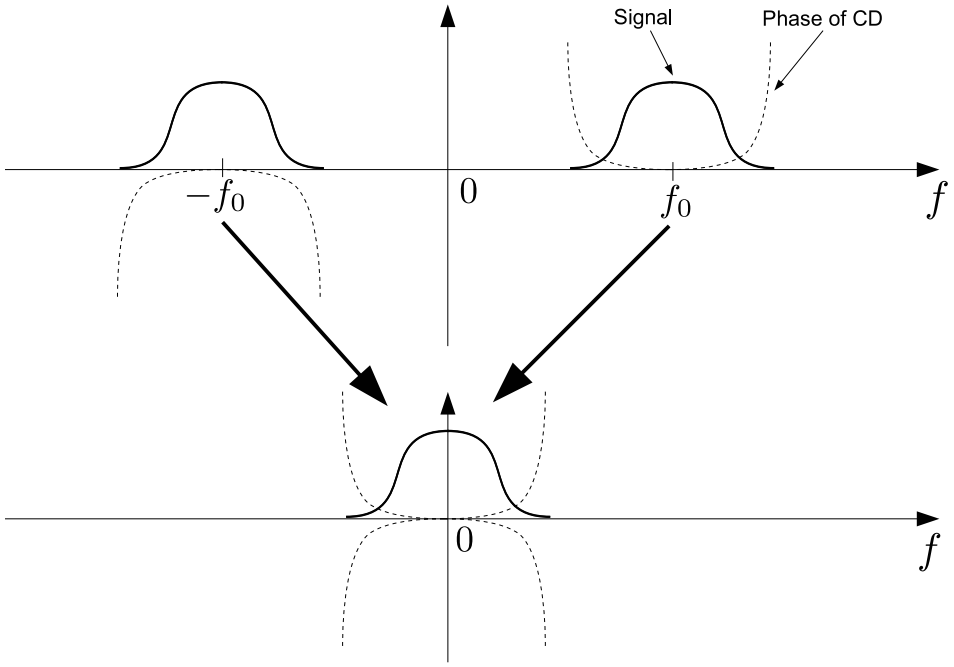

Figure 2.8: Effect of chromatic dispersion in a non-coherent system

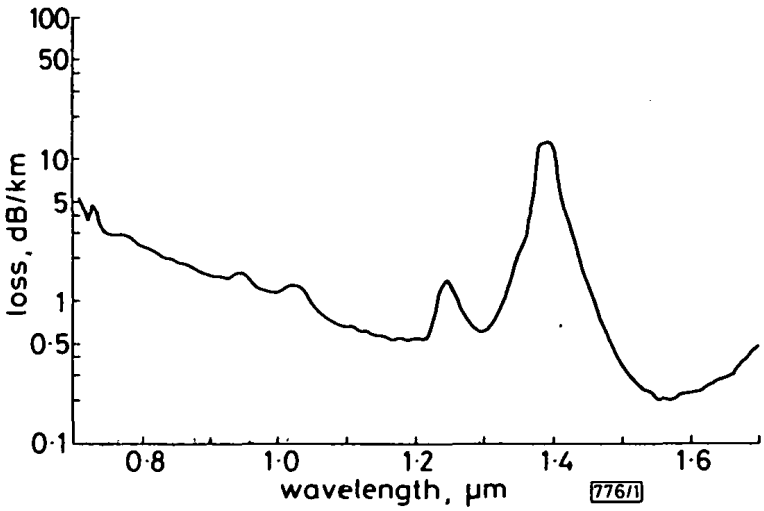

Figure 2.9: Attenuation profile of SSMF (from [24])

Band	Description	Range (nm)	Range (THz)
O-band	Original	1260 to 1360	237.9 to 220.4
E-band	Extended	1360 to 1460	220.4 to 205.3
S-band	Short wavelength	1460 to 1530	205.3 to 195.9
C-band	Conventional	1530 to 1565	195.9 to 191.6
L-band	Long wavelength	1565 to 1625	191.6 to 184.5
U-band	Ultra-long wavelength	1625 to 1675	184.5 to 179.0

Table 2.1: Single-mode spectral bands [15]

The band with the lowest attenuation is C-band, which is also the operation band of the most common optical amplifier, the EDFA, and is the band employed by regional and long-haul networks. Another common band is O-band, which has a low attenuation and, for SSMF, has the lowest chromatic dispersion, therefore is widely employed in access and short reach metro networks. E-band has a strong attenuation peak due to presence of water (*water peak*), but a special manufacturing process can remove it, creating Zero Water Peak (ZWP) fiber, allowing the use of this band.

2.5.3 Optical amplification

In order to recover amplitude in optical transmission systems, *optical amplifiers* are employed, which increase the signal power in all-optical domain.

Erbium Doped Fiber Amplifiers

The most common optical amplifier for C-band signals is the EDFA [1, ch.7]. An EDFA is made by a short span (few meters) of optical fiber doped with erbium (Er^{3+}), where together with the signal a laser pump is added with a Wavelength Division Multiplexing (WDM) coupler; this creates a population inversion in the fiber, creating an optical amplification effect. The most common pump wavelength is 980 nm (305.9 THz).

EDFAs have a large bandwidth[3], and with a gain flattening filter it can have an almost constant gain all over the amplification bandwidth. An EDFA adds random white Gaussian noise, flat across all the amplifier bandwidth, called ASE, with Power Spectral Density (PSD)

$$\Psi_{\text{ase}}(f) = n_{\text{sp}} h f_0 (G - 1)$$

$h = 6.63 \times 10^{-34}$ J s is Planck's constant, f_0 the central frequency of the amplified signal, G the gain and $n_{\text{sp}} > 1$ the *spontaneous emission factor*, which for $G \gg 1$ is related to the noise figure of the amplifier with a simple expression $n_{\text{sp}} \approx \frac{1}{2} F_{\text{n}}$.

The main drawback of the EDFA is that it can amplify only C-band signals (and, with some modifications, L-band), and that is why C-band is the most common band used for long haul transmission.

[3]For instance, the EDFA used in this experiment (Oclaro PureGain PG1600) has a bandwidth of 35 nm (4.4 THz) with a gain of 23 dB

Semiconductor Optical Amplifiers

Another kind of optical amplifiers is the Semiconductor Optical Amplifier (SOA). An SOA is a semiconductor laser with an anti-reflective coating on the facets and two isolators before and after the diode.

These kind of amplifiers are less common because they exhibit strong non-linear effect, such as Cross Gain Modulation (XGM) and Cross Phase Modulation (XPM), and have a worse noise with respect to EDFAs, but they can be integrated in the transceiver.

2.6 Single Sideband

As we saw in the previous section, chromatic dispersion will irreversibly degrade the performance of a self-coherent system, so this problem cannot be solved at the receiver, as we do with coherent systems. The only solution is changing the transmit signal in order to make it resilient from chromatic dispersion.

The solution we adopted in this work is transmitting a SSB signal, which, as we will see later, is (in principle) unaffected by chromatic dispersion.

2.6.1 Definition

Real signals have the Hermitian property (A.1), which means that only half of the spectrum contains information and the other half is just a copy, so if we can tolerate to have a complex signal in baseband, we can *remove* half of the spectrum without any loss of information. This can be done by adding to the real signal $s(t)$ an imaginary part which is the *Hilbert transform* of the signal

$$s_{\text{ssb}}(t) = \frac{1}{2}\left[s(t) + j\,\mathcal{H}\{s(t)\}\right] \tag{2.6}$$

where the Hilbert transform is a linear all-pass filter that has a phase of $-\pi/2$ for positive frequencies and a phase of $\pi/2$ for negative frequencies (the DC gain is conventionally set to 0, but in almost all practical implementations the $s(t)$ does not have a DC component)

$$\begin{gathered}\mathcal{H}\{s(t)\} = s(t) \otimes h_{\mathcal{H}}(t) \qquad \forall s(t) \in \Re \\ h_{\mathcal{H}}(t) = \frac{1}{\pi t} \xrightarrow{\mathcal{F}} H_{\mathcal{H}}(f) = \begin{cases} -j & f > 0 \\ +j & f < 0 \\ 0 & f = 0 \end{cases}\end{gathered} \tag{2.7}$$

It is easy to see that $\mathcal{H}\{s(t)\} \in \Re$, so $j\,\mathcal{H}\{s(t)\}$ is imaginary. The spectrum of the SSB signal therefore is

$$S_{\text{ssb}}(f) = \begin{cases} S(f) & f \geq 0 \\ 0 & f < 0 \end{cases}$$

The signal is using half of the bandwidth, without any loss of information since the original signal can be reconstructed by taking the real part of the SSB signal

$$s(t) = 2\Re\{s_{\text{ssb}}(t)\}$$

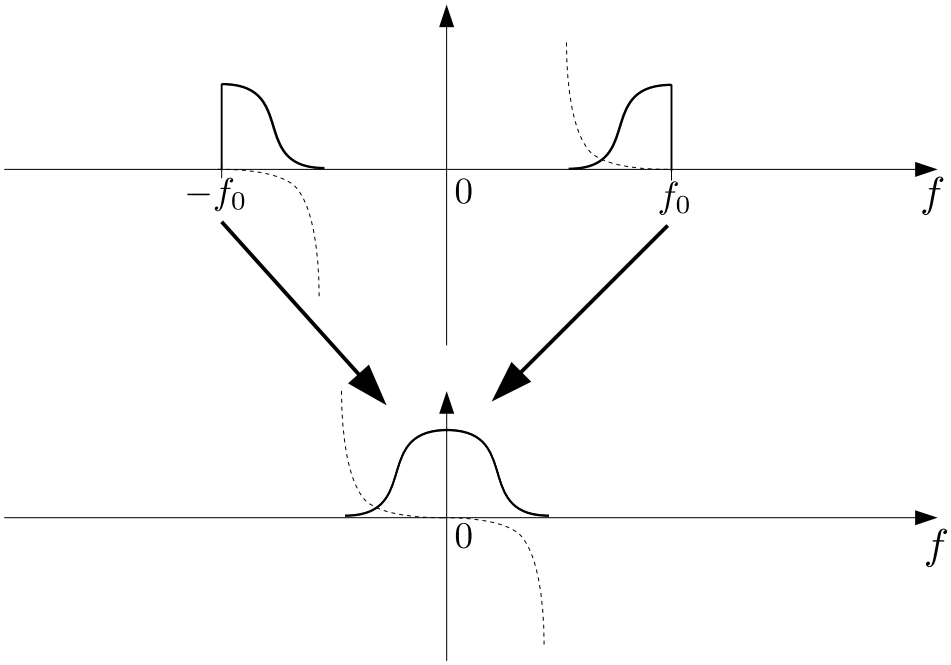

Figure 2.10: Effect of chromatic dispersion to an SSB signal

2.6.2 SSB and chromatic dispersion

The effect of an SSB signal to the signal-carrier beating in a self-coherent system can be seen in Figure 2.10, where the baseband signal is not anymore the sum of two components but takes the first half of the specrum from the positive frequencies and the other half from the negative frequencies, so any phase difference will not create destructive interference.

In complex baseband, assuming an SSB optical field $e_{\text{ssb}}(t) = e(t) + j\,\mathcal{H}\{e(t)\}$, we get

$$E_{\text{ssb}}(f)e^{-j\beta_2 f^2 d/2} + E^*_{\text{ssb}}(-f)e^{j\beta_2 f^2 d/2} = \begin{cases} E_{\text{ssb}}(f)e^{-j\beta_2 f^2 d/2} & f \geq 0 \\ E^*_{\text{ssb}}(-f)e^{j\beta_2 f^2 d/2} & f < 0 \end{cases} = \\ = E(f) \cdot e^{-j\,\text{sgn}(f)\beta_2 f^2 d/2}$$

which is the original signal $e(t)$ affected by an all-pass filter that can be compensated using an equalizer.

This is a known technique, which has already been applied in the past to other modulation formats [44] and recently applied to DMT in [45], which represents the best way to reduce the impact of chromatic dispersion in C-band over SSMF.

We performed a more detailed study of the impact of transmitter imperfections on SSB signals, discussed in chapter 5.

Chapter 3

Discrete Multitone

In the previous chapter we introduced optical SSB self-coherent systems as a trade-off between complexity and efficiency, and we adopted a real modulation format. In this chapter we will introduce two real modulation formats suitable for these kind of systems: Pulse Amplitude Modulation (PAM) and DMT. Then we will discuss more in detail DMT since it is the system adopted in this work. The main references used throughout this chapter are [4, 29].

3.1 Digital communication systems

Throughout this chapter we assume the very simple system model shown in Figure 3.1. At the transmitter the *modulator* maps bits from the source to one of the M complex symbols in the symbol set

$$\mathcal{S} = \left\{ s^{(1)}(t), s^{(2)}(t), \ldots, s^{(M)}(t) \right\}$$

and transmits one of them every T seconds over the channel, leading to a transmitted signal

$$x(t) = \sum_{\ell=-\infty}^{+\infty} s_\ell(t - \ell T)$$

where $s_\ell(t)$ is the ℓ-th transmitted symbol. T is called *symbol time* and its inverse $R_\mathrm{s} = 1/T$ is called *symbol rate* and it is measured in *baud* (Bd).

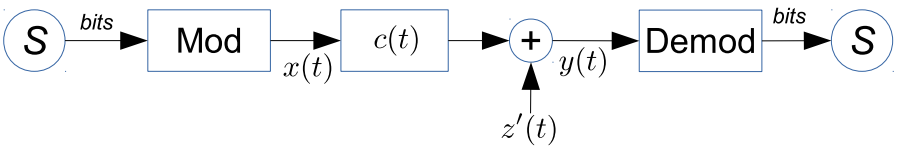

Figure 3.1: Digital transmission system model

The channel is represented as a linear time-invariant filter with impulse response $c(t)$ and a *bandwidth* B, *i.e.* its power spectral density is nonzero only for $|f| \leq B/2$; then an Additive White Gaussian Noise (AWGN) process $z'(t)$ is added to the output of the filter.

The receiver receives a signal $y(t)$ from the channel, and the *demodulator* will estimate the sequence of symbols that has been transmitted. Then it will map them to a sequence of bits and send it to the sink.

The main performance indicator of a digital communication system is the BER, which is the ratio between the wrong bits and the total transmitted bits. In the design of a communication systems is often defined a *target BER*, and if the BER gets higher than the target BER we say that the system is *out of service*.

3.2 Single channel modulation

3.2.1 Transmitter

The most simple real modulation format is called PAM. With this modulation format we transmit a sequence of independent discrete symbols $\{a[n]\}_{n=-\infty}^{+\infty}$ with power σ_a^2 taken from an alphabet

$$\mathcal{A} = \{-(M-1), -(M-1)+2, \ldots, (M-1)-2, M-1\}$$

that contains M symbols. The *mapper* maps $\log_2(M)$ bits to one of the symbols, which is then used to modulate the amplitude of a pulse $p(t)$, leading to a transmit signal

$$x(t) = \sum_{n=-\infty}^{+\infty} a[n]p(t-nT)$$

so the symbol set is

$$s(t) = \{a[k]p(t)\} \quad a[k] \in \mathcal{A}$$

with a bit rate

$$R_\mathrm{b} = \frac{\log_2(M)}{T} \tag{3.1}$$

3.2.2 Receiver

After the channel, the receiver will filter the input signal with a receive filter $r(t)$ and sample it every T seconds

$$y[n] = \big[(x(t) \otimes c(t) + z'(t)) \otimes r(t)\big]_{t=nT} = a[n] \otimes h[n] + z[n] \tag{3.2}$$

where $h[n]$ is an equivalent discrete-time filter that takes into account the pulse-shaping filter, channel and receive filter

$$h[n] = [p(t) \otimes c(t) \otimes r(t)]_{t=nT} \tag{3.3}$$

and $z[n]$ is the additive noise $z'(t)$ sampled and filtered with $r(t)$. The demodulator will then estimate the sequence $a[n]$ from $y[n]$, leading to an estimated sequence $\hat{a}[n]$.

The model of the discrete-time PAM channel is shown in Figure 3.2.

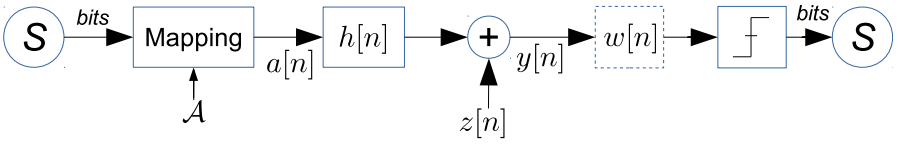

Figure 3.2: Discrete-time model for PAM

3.2.3 Channel memory

In all cases of practical interest $h[n]$ has a limited *channel memory* δ, *i.e.* $h[n] \neq 0$ only for $n = 0, \ldots, \delta$. The value of δ depends on the three impulse responses $p(t)$, $c(t)$ and $r(t)$. To predict its impact, let us consider the simplest case where $c(t) = \delta(t)$, *i.e.* the channel is ideal.

Ideal channel

If we want to have zero memory, we have to satisfy this condition

$$[p(t) \otimes r(t)]_{t=nT} = \delta[n]$$

which translates in the Discrete Time Fourier Transform (DTFT) domain to the popular Nyquist's criterion [26]

$$H\left(e^{j2\pi fT}\right) = \frac{1}{T} \sum_{n=-\infty}^{+\infty} P(f - n/T)R(f - n/T) = 1 \tag{3.4}$$

It is trivial to note that a waveform *must* have a bandwidth at least $1/T = B_{\min}$ to satisfy (3.4), and this is called the *minimum bandwidth* of the system. Usually transmission systems do not work at the minimum bandwidth, since the only pulse possible is the sinc pulse

$$p(t) \otimes r(t) = \operatorname{sinc}(t/T)$$

which is difficult to implement; moreover, this makes timing recovery at the receiver very difficult. Communication systems usually transmit with a bandwidth $B = B_{\min}(1 + \rho)$, where $\rho \geq 0$ is the *excess bandwidth* factor. Common values of ρ are between 0.2 and 0.3.

Non-ideal channel

Let us now consider a non-ideal channel impulse response $c(t) \neq \delta(t)$; in this case there are two possible cases, depending on the shape of $C(f) = \mathcal{F}\{c(t)\}$

- $C(f) \approx 1$ for $|f| \leq 1/2T$, this means that the DTFT of the overall impulse response is almost flat $H\left(e^{j2\pi fT}\right) \approx h[0]T$ and we can approximate the impulse response $h[n] = h[0]\delta[n]$ with a single pulse. This means that $\delta = 0$ and the channel is *memoryless*

- $C(f)$ changes rapidly for $|f| \leq 1/2T$, this means that the DTFT of the overall impulse response $H\left(e^{j2\pi fT}\right)$ is not flat and the impulse response $h[n]$ has a length $\delta > 0$; in this case we say that the channel has memory.

Channel memory creates an effect called Intersymbol Interference (ISI), since the received signal

$$y[n] = h[n] \otimes a[n] = \sum_{i=0}^{\delta} h[i]a[n-i]$$

is the n-th symbol, which we want to receive, affected by the previous δ symbols, and this makes difficult the estimation of the transmitted symbol $a[n]$.

It is interesting to see that the memory depends on the shape of $C(f)$ with respect to the inverse of the symbol rate $1/T$, so a possible remedy for ISI could be the increase of T,. However, in single-channel systems the overall bitrate linearly depends on $1/T$ (3.1), hence the increase of T is not a feasible option. The most common remedy is the application of a linear filter $w[n]$ at the receiver called *linear equalizer* which tries to reduce ISI at the receiver before detection.

3.2.4 Signal-to-noise ratio

It is interesting to see that the zero-ISI constraint of (3.4) for an ideal channel is not on $p(t)$ and $r(t)$, but on their convolution, which means that we have another degree of freedom in the choice of these two filters.

The second constraint can be the maximization of the Signal-to-Noise Ratio (SNR) after the sampling. If we assume that $\Psi_{z'}(f) = N_0$, and we are transmitting only one symbol at $t = 0$ the power of the noise after sampling is

$$P_{\mathrm{n}} = T \int_{-1/2T}^{+1/2T} \Psi_{z'}(e^{j2\pi fT}) \left|R(e^{j2\pi fT})\right|^2 \mathrm{d}f = N_0 E_{\mathrm{r}}$$

where E_{r} is the energy of the filter $r(t)$ sampled every T seconds; the power of the signal is

$$P_{\mathrm{sig}} = \sigma_a^2 \left|[p(t) \otimes r(t)]_{t=0}\right|^2 = \sigma_a^2 \left| \int_{-\infty}^{+\infty} p(\tau) r(-\tau)\, \mathrm{d}\tau \right|^2 \leq \sigma_a^2 E_{\mathrm{p}} E_{\mathrm{r}}$$

where the last inequality is Schwarz inequality. Therefore

$$\mathrm{SNR} = \frac{P_{\mathrm{sig}}}{P_{\mathrm{n}}} \leq \frac{\sigma_a^2 E_{\mathrm{p}}}{N_0}$$

and the equality holds for $r(t) = p^*(-t)$, called *matched filter* to $p(t)$.

It is important to note that this result holds only for ideal channels, although it can be proven that for non-ideal channels the matched filter followed by sampling every T seconds is a sufficient statistics to recover the maximum SNR for that specific channel

[4, p.165]. It can also be proven [4, 10] that the best infinite-length *linear* equalizer can get an SNR which is the *arithmetic mean* of the input SNRs at each frequency

$$\mathrm{SNR}_{\mathrm{LE}} = \sigma_a^2 \left[T \int_{-1/2T}^{1/2T} \frac{\Psi_z\left(e^{j2\pi fT}\right)}{\Psi_h\left(e^{j2\pi fT}\right)} \,\mathrm{d}f \right]^{-1} \tag{3.5}$$

where $\Psi_z(f)$ and $\Psi_h(f)$ are (respectively) the Power Spectral Densities (PSDs) of the noise $z[n]$ and the channel filter $h[n]$.

In an optical communication system the channel has always memory, and this is mainly due to the limited bandwidth of the components used in the system. Since our goal is the reduction of the cost of a communication system, we will have to deal with limited bandwidth components, so PAM is not the optimal solution to deal with strong ISI.

3.3 Multichannel modulation

As we have seen in the section before, the channel memory mainly depends on the shape of $H(f)$ compared with the symbol rate, so one possible solution to avoid ISI would be reducing the symbol rate. The problem with PAM is that the bit rate (3.1) linearly depends on the symbol rate, so an increase of T will necessary mean a decrease of the bit rate with the same SNR. The only way to achieve this is to use a completely different transmission scheme, and one possible solution is *multichannel modulation*.

In a multichannel modulation we divide the transmit bits into N independent channels, called *subchannels*, map them into symbols drawn from an alphabet, and transmit all the N symbols together every NT seconds. In this case we have a symbol rate of $1/(NT)$ but a bit rate which is the sum of the bitrates of the channels, and if N is chosen big enough we will have a memoryless multi-channel system with the same bitrate of a single-channel system with the same bandwidth.

3.3.1 General model

Let us consider the general model in figure 3.1. As we stated before, the channel has bandwidth B, so $C(f) = 0$ for $|f| > B/2$, and with this in mind let us divide the transmit channel in the frequency domain into N subchannels, each with bandwidth B_k and center frequency f_k for $k = 0, \ldots, N-1$.

The structure of a multichannel transceiver is shown in Figure 3.4. The encoder maps the input bits into the N channels with a symbol $a[k]$ drawn from a complex alphabet $\mathcal{A}_k$ (*e.g.* Quadrature Amplitude Modulation (QAM)). Each of these symbols is transformed every NT seconds into a continuous-time signal using a pulse-shaping filter $\varphi(t)$, where $T = 1/B$, and multiplied by a carrier with frequency f_k. All the signals are summed together getting a transmit signal $x(t)$, which is sent to the channel linear filter with impulse response $h(t)$ with the addition of an AWGN process $z(t)$. The receiver will divide the received signal into N paths, and in each of them the signal is multiplied with

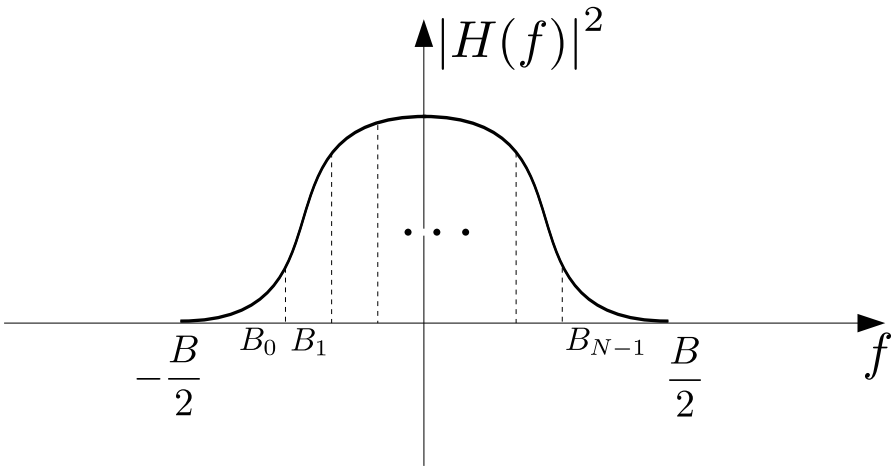

Figure 3.3: Multichannel modulation

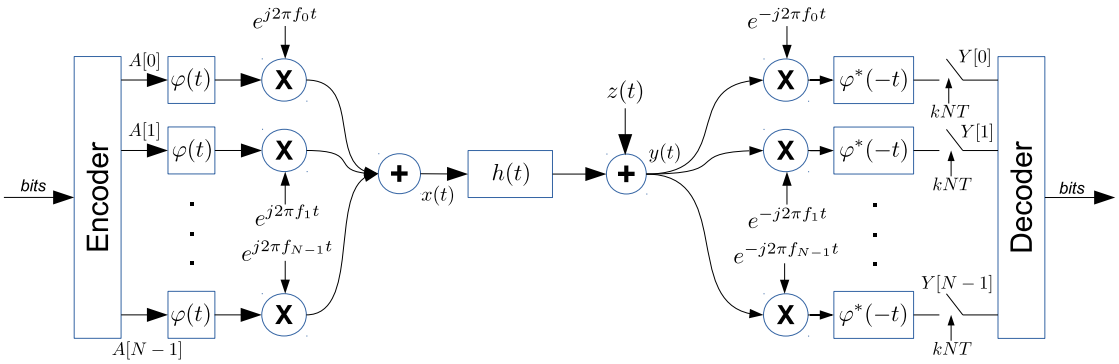

Figure 3.4: Multichannel transceiver (adapted from [9])

a carrier with frequency $-f_k$, filtered by the matched filter $\varphi^*(-t)$, sampled every NT seconds and sent to the decoder that recovers the original transmitted sequence.

3.3.2 Orthogonal Frequency Division Multiplexing

The main application of multichannel modulation is called OFDM. In this case, the transmit channel is *uniformly* divided into N subchannels, so that the subchannels center frequencies are

$$f_k = \frac{k}{NT} \qquad k = -N/2, \ldots, N/2 - 1$$

and the symbol set is

$$\mathcal{S} = \left\{ \sum_{k=0}^{N-1} A[k] \sqrt{\frac{1}{NT}} \operatorname{rect}\left(\frac{t}{NT}\right) e^{j2\pi tk/(NT)} \right\} \qquad A[k] \in \mathcal{A} \tag{3.6}$$

The main property of this scheme is that every symbol in the symbol set is *orthogonal* in frequency

$$\left\langle e^{j2\pi tk/(NT)}, e^{j2\pi tn/(NT)} \right\rangle = \frac{1}{NT} \int_{-NT/2}^{NT/2} e^{-j2\pi tk/(NT)} e^{j2\pi tn/(NT)} \, \mathrm{d}t = \delta[n-k]$$

which means that all the N subcarriers form an orthonormal basis, so the decoder is simply *projecting* the received signal onto the orthonormal basis to recover the subcarriers.

Discrete-time implementation

One of the reasons why OFDM is popular is its discrete-time implementation. For the following calculations, we will consider the transmission of one *OFDM block*, that is only one element of the symbol set.

This implementation uniformly samples the transmit block $s(t) \in \mathcal{S}$ every T seconds, getting a discrete signal

$$s[n] = \sqrt{\frac{1}{N}} \sum_{k=0}^{N-1} A[k] e^{j2\pi nk/N}, \quad n = 1, \ldots, N-1 \tag{3.7}$$

which is transmitted over a channel using a pulse-shaping filter $p(t)$

$$x(t) = \sum_{n=-\infty}^{+\infty} s[n] p(t - nT) \tag{3.8}$$

The receiver will filter the signal using a receive filter $r(t)$ and sample it again every T seconds

$$y[n] = [y(t) \otimes r(t)]_{t=nT} = x[n] \otimes h[n]$$

where $h[n]$ is the equivalent-discrete time channel described in equation (3.3), with memory δ samples.

We then separate the subchannels by projecting the signal over the orthonormal basis used to transmit it (3.7)

$$Y[k] = \sqrt{\frac{1}{N}} \sum_{n=0}^{N-1} y[n] e^{-j2\pi nk/N}, \quad k = 1, \ldots, N-1 \tag{3.9}$$

The transmitted symbols can be estimated from each subcarrier after some additional processing (*e.g.* equalization, carrier recovery, hard decision,...), depending on the channel

$$Y[k] \to \hat{A}[k]$$

We first see that the operations in (3.9) and (3.7) are (respectively) the Discrete Fourier Transform (DFT) and the Inverse DFT (IDFT); for $N = 2^n$ they can be implemented using the efficient Fast Fourier Transform (FFT) algorithm. Additionally, the modulation and demodulation operations can be executed in parallel over an entire OFDM block, requiring, in hardware, only $1/N$ of the clock speed of an equivalent single-channel system.

Equalization

Since the signal is generated in the frequency domain, it is more efficient if the equalization of the signal is performed block-wise in the frequency domain. Thanks to the relation

$$X[k] \cdot H[k] \iff x[n] \underset{\mathrm{C}}{\otimes} h[n] \qquad n, k = 0, \ldots, N-1$$

we can perform this, but the convolution on the right is not a regular (linear) convolution, but it is the so-called *circular* convolution, *i.e.* is a convolution performed over N samples where the signal x is periodically repeated with period N.

Additionally, in the previous section we considered the transmission of only one block. Let us now consider an infinite sequence of blocks

$$x[n] = \sum_{\ell=-\infty}^{+\infty} s_\ell[n - \ell N]$$

where $s_\ell[n]$, for $n = 0, \ldots, N-1$ and zero everywhere else, is the ℓ-th OFDM block.

After transmission over the equivalent discrete-time channel $h[n]$ we get

$$y[n] = x[n] \otimes h[n] = \sum_{i=0}^{\delta} h[i] x[n-i]$$

In this case we see that each sample affects the next δ samples regardless of its position inside the block. For instance, the 1^{st} sample in the block $\ell = 1$ $y[N]$ is affected by the previous δ samples $x[N-\delta], x[N-\delta+1], \ldots, x[N-1]$ which belong to the previous block

($\ell = 0$), leading to an effect called Interblock Interference (IBI). This effect forbids us to equalize the channel in the frequency domain block-wise using a Frequency Domain Equalizer (FDE)

$$\hat{A}_\ell[k] = W[k]Y_\ell[k]$$

There are two possible solutions:

- Adopt an adaptive equalizer using an algorithm like *overlap-save* or *overlap-add* that allows the use of FDE over linear channels; this will increase the complexity of the system because needs an additional FFT and Inverse FFT (IFFT), plus the additional components to perform coefficient adaptation and the overlap.
- Add a *guard interval* of length $\geq \delta$ between adjacent blocks, losing spectral efficiency.

The most common solution is the second, where we accept to lose some spectral efficiency to have an efficient equalization mechanism.

The guard interval, as stated before, is a known (by the receiver) sequence of $N_\mathrm{c} \geq \delta$ samples inserted between blocks that cancels out the IBI. The samples of this sequence cannot be random, but they must be accurately chosen to fulfill the aforementioned circular convolution constraint. This is achieved by *repeating* the first N_c samples of the block at the end of the block, leading to a transmit signal

$$\ldots, s_\ell[0], s_\ell[1], \ldots, s_\ell[N-1], \underbrace{s_\ell[0], s_\ell[1], , \ldots, s_\ell[N_\mathrm{c}-1]}_{\text{cyclic prefix}}, s_{\ell+1}[0], \ldots$$

where the guard interval takes the name of *cyclic prefix* or *cyclic extension*. The cyclic prefix will decrease the spectral efficiency by a factor of

$$\eta_\mathrm{cp} = \frac{N}{N + N_\mathrm{c}}$$

Usually the cyclic prefix length is measured as a ratio between its length and the total length of the block, called *cyclic prefix overhead*, and often measured as a percentage

$$\mathrm{OH}_\mathrm{cp} = \frac{N_\mathrm{c}}{N + N_\mathrm{c}} = 1 - \eta_\mathrm{cp}$$

By applying this method the receiver, for each block, discards the cyclic prefix, performs the FFT operation and applies the FDE.

3.3.3 Discrete Multitone

In the previous section we described the OFDM system, but there is one problem left to tackle: *it is not a real modulation format*. The output of an IDFT, described in equation (3.7), in general is a complex number being the weighted sum of complex exponentials.

The transmit signal $s[n]$ can be made real by imposing the *Hermitian symmetry* in the frequency-domain signal $A[k]$, that is setting half of it as the mirrored and conjugated copy of the others.

In math, let us write equation (3.7) as the IDFT of the sequence $S[k]$, with some other small modifications

$$s[n] = \sqrt{\frac{1}{N}} \sum_{k=0}^{N-1} g_k S[k] e^{j2\pi nk/N} \tag{3.10}$$

where the sequence $S[k]$ is defined as

$$S[k] = \begin{cases} A[k] \in \mathcal{A}_k & k = 1, \ldots, N/2 - 1 \\ A^*[N-k] & k = N/2 + 1, \ldots, N - 1 \\ 0 & \text{otherwise} \end{cases} \tag{3.11}$$

In this definition we note few things:

- N is assumed even, but since in all cases of practical interest N is a power of two, this is a reasonable assumption.
- We do not transmit anymore N complex symbols, but $N/2 - 1$, losing more than half of the spectral efficiency. For the DC ($k = 0$) and Nyquist ($k = N/2$) frequencies, we can put a real symbol (*e.g.* PAM), which would correspond to an extra complex symbol that can increase the number of complex symbols to $N/2$ (losing exactly half of the spectral efficiency); in real channels usually the DC and the Nyquist are not modulated, and that's why they are set to zero.
- The symbol alphabet $\mathcal{A}_k$ is different among the subcarriers, allowing to allocate a different number of bits in each subcarrier (*bit loading*).
- We also introduced a pre-emphasis factor g_k which can be used to allocate different powers to different subcarriers (*power loading*).

A system with these properties takes the name of *Discrete Multitone*, which is a variant of the discrete-time implementation of OFDM. The possibility of changing the modulation format and the gain for each subcarrier can be exploited to get closer to the channel capacity, and this will be discussed in details in the next chapter.

SSB-DMT

Since DMT is a real modulation format, we can transmit only one sideband (SSB), described in section 2.6. This will recover the spectral efficiency, achieving the same as OFDM, and at the same time will make the system resistant to chromatic dispersion. The main drawback is the requirement of a transmitter capable of transmitting a complex signal, increasing its complexity (and cost).

From a theoretical standpoint the SSB equation (2.6) can be combined with (3.11) to get the DMT-SSB equation

$$S_{\text{ssb}}[k] = \begin{cases} A[k] \in \mathcal{A}_k & k = 1, \ldots, N/2 - 1 \\ 0 & \text{otherwise} \end{cases} \tag{3.12}$$

therefore we can efficiently generate the signal in the frequency domain without applying a Hilbert filter.

Chapter 4

Capacity

In the previous section we described DMT modulation, comparing it with single-channel modulation formats such as PAM. We provided in (3.5) the important result of the maximum SNR for single channel systems with linear equalization, but we did not provide a similar result for DMT since depends on the choice of the gain and modulation scheme in each subcarrier. In this chapter we will discuss in detail the capacity of a multichannel system, finding the expression of the maximum SNR for multi-channel systems, and we will provide a practical algorithm to optimally allocate bits and powers amongst subcarriers. The main reference used throughout this chapter is [9].

4.1 Capacity of a multichannel system

Let us consider the channel model described in section 3.3.1, where we assume that the AWGN process $z(t)$ has a PSD N_0, and for the moment let us consider as channel input the signal $x(t)$ and as channel output $y(t)$ (neglecting the multichannel modulation and demodulation). The capacity of this channel is given by Shannon's formula [36]

$$C = \int_{-B/2}^{B/2} \log_2 \left(1 + \frac{|H(f)|^2}{N_0 B}\right) \mathrm{d}f = \int_{-B/2}^{B/2} \log_2 \left[1 + \mathrm{SNR}(f)\right] \mathrm{d}f$$

where we defined as channel SNR the quantity

$$\mathrm{SNR}(f) = \frac{|H(f)|^2}{N_0 B}$$

We assume that the SNR is a property of the channel, *i.e.* is a quantity that we *cannot control*.

Let us now consider the entire multichannel system, where the channel is divided into N subchannels as shown in Figure 3.3, and we introduce the fundamental assumption that N is big enough to have a memoryless system; this means that

$$|H(f)|^2 \approx |H[n]|^2 \qquad f \in B_n, \quad \forall n = 0, \dots, N-1 \tag{4.1}$$

so this is like having N independent AWGN channels with no memory

$$Y[n] \approx X[n]A[n] + Z[n]$$

and the capacity becomes the sum of the capacities of the subchannels

$$C = \sum_{n=0}^{N-1} B_n \log_2 (1 + \mathrm{SNR}[n])$$

with SNR per subchannel

$$\mathrm{SNR}[n] = \frac{|H[n]|^2}{N_0 B_n} \tag{4.2}$$

Let us consider now only the n-th subcarrier. Its capacity, in bits per complex dimension, is

$$c_n = \log_2 (1 + \mathrm{SNR}[n])$$

and represents the maximum number of bits that we can reliably transmit on this subchannel.

4.1.1 SNR gap

In a real system we cannot transmit at the channel capacity, but we can transmit at a lower rate, which can be written as

$$\bar{b}_n = \log_2 \left(1 + \frac{\mathrm{SNR}[n]}{\Gamma_n} \right) \tag{4.3}$$

bits, with $\Gamma_n \geq 1$.

Γ_n is called *SNR gap*, which is a convenient mechanism to relate channel capacity and achievable bit rate. The SNR gap depends on the modulation format, coding scheme, and maximum acceptable bit error rate tBER.

In order to define the SNR gap Γ_n we first have to define another function, the *required SNR*. The required SNR $r\mathrm{SNR}(\bar{b}_n)$ is the minimum SNR needed, for a given modulation and coding scheme with $\bar{b}_n$ bits per dimension, to have a bit error rate lower or equal than tBER in a given channel. The SNR gap is then defined as the ratio between the required SNR and the minimum SNR needed to have a capacity of $\bar{b}_n$ bits per dimension

$$\Gamma_n = \frac{r\mathrm{SNR}(\bar{b}_n)}{2^{\bar{b}_n} - 1}$$

For example, for uncoded square M-QAM constellation the SNR gap can be conveniently calculated by inverting the BER curves, shown in Figure 4.1.

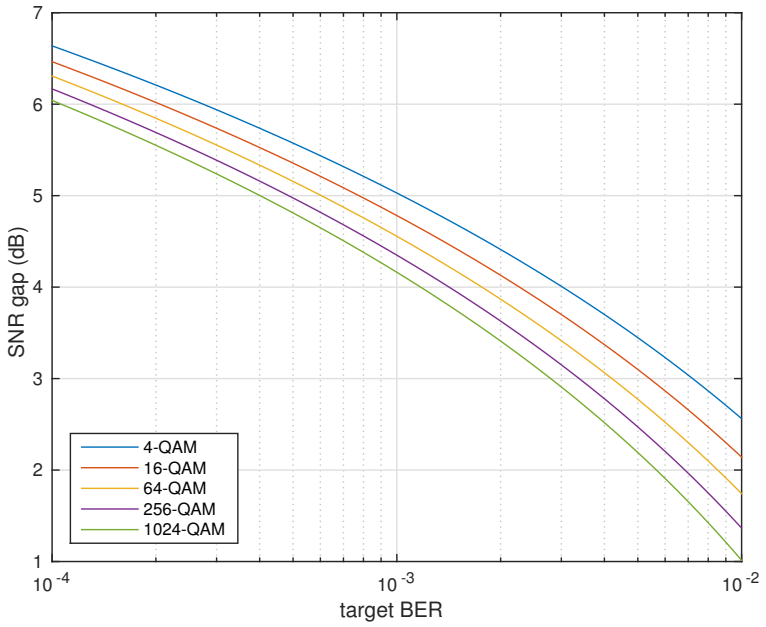

Figure 4.1: SNR gap for uncoded square M-QAM constellations

4.1.2 SNR margin

Let us now consider the DMT channel, where the signal is transmitted according to equation (3.10). The main difference with (4.3) is the inclusion of a gain factor g_n, becoming

$$\bar{b}_n = \log_2\left(1 + |g_n|^2 \frac{\mathrm{SNR}[n]}{\Gamma_n}\right)$$

In a real system usually we do not want to transmit exactly $\bar{b}_n$ in every subcarrier for two main reasons.

- The total bit rate
$$R_\mathrm{b} = \frac{1}{T}\sum_{n=0}^{N-1} \bar{b}_n = \frac{N_\mathrm{bb}}{T}$$
in optical communication systems is a fixed value and cannot be changed arbitrarily.

- The exact SNR per subchannel is usually unknown and must be estimated, so in case of an estimation error where the real SNR is lower than the estimated value, we may have a system outage.

For these two reasons we usually choose to transmit $b_n \leq \bar{b}_n$ bits per subcarrier,

defined as

$$b_n = \log_2\left(1 + |g_n|^2 \frac{\mathrm{SNR}[n]}{\Gamma_n \lambda_n}\right)$$

where $\lambda_n \geq 1$ is called *SNR margin*, and represents the maximum amount by which $\mathrm{SNR}[n]$ can decrease while keeping the bit error rate $\mathrm{BER}[n]$ lower than the target BER.

The average number of bits per DMT symbol is

$$\langle b \rangle = \frac{1}{N}\sum_{n=0}^{N-1} b_n = \frac{1}{N}\sum_{n=0}^{N-1} \log_2\left(1 + |g_n|^2 \frac{\mathrm{SNR}[n]}{\Gamma_n \lambda_n}\right) =$$
$$= \frac{1}{N}\log_2\left[\prod_{n=0}^{N-1}\left(1 + |g_n|^2 \frac{\mathrm{SNR}[n]}{\Gamma_n \lambda_n}\right)\right] = \log_2\left(1 + \mathrm{SNR}_{\mathrm{mc}}\right)$$

In this case the multichannel bit rate can be seen as the bit rate of a single-channel AWGN system with no ISI with an equivalent multichannel SNR defined as

$$\mathrm{SNR}_{\mathrm{mc}} \triangleq \left[\prod_{n=0}^{N-1}\left(1 + |g_n|^2 \frac{\mathrm{SNR}[n]}{\Gamma_n \lambda_n}\right)\right]^{1/N} - 1$$

Assuming high SNR values, the $+1$ can be ignored leading to the *geometric SNR*

$$\mathrm{SNR}_{\mathrm{mc}} \approx \left[\prod_{n=0}^{N-1}\left(|g_n|^2 \frac{\mathrm{SNR}[n]}{\Gamma_n \lambda_n}\right)\right]^{1/N}$$

It is interesting to compare this result with the result provided in (3.5) for the best linear equalizer. According to Jensen's inequality, the geometric SNR is always greater or equal than arithmetic SNR, which means that a DMT with an optimal choice of b_n and g_n can outperform the best possible linear equalizer for single-channel modulation. The geometric SNR can be reached in single-channel modulation by adopting an optimal infinite-length Zero-Forcing (ZF)-DFE [10], which is a non-linear equalizer, with the main drawback of requiring a low-latency feedback loop which is difficult to design in high-speed links.

4.2 Allocation policies

In order to achieve the capacity described in the previous subsection, we need to optimally choose the number of bits and the pre-emphasis factor for each subcarrier, given the channel SNR.

There are two main ways to proceed, depending on the system design goals.

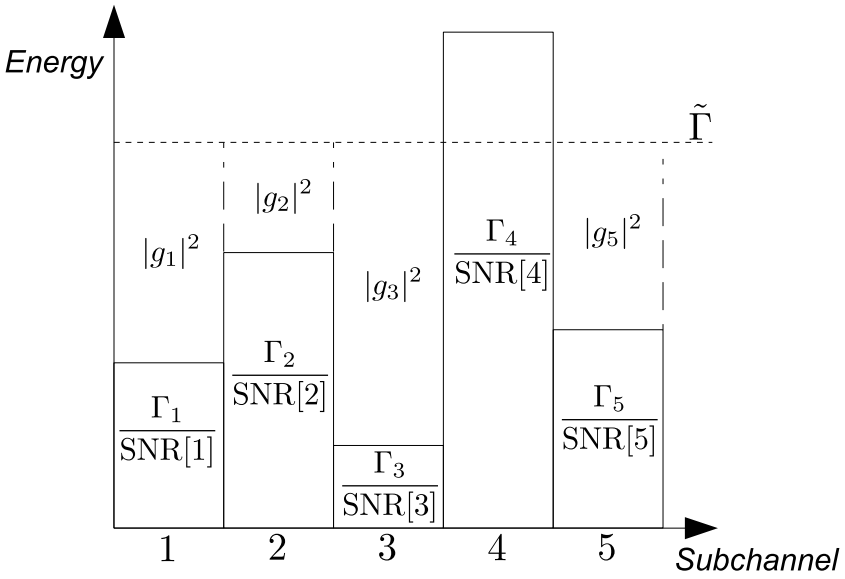

Figure 4.2: Rate Adaptive water filling

4.2.1 Rate Adaptive

This first approach tries to maximize the total bit rate

$$\max_{|g_n|^2} \left\{ \sum_{n=0}^{N-1} b_n \right\}$$

with a total transmit energy constraint

$$\text{subject to} \quad \sum_{n=0}^{N-1} |g_n|^2 = \mathcal{E}$$

The solution, using Lagrange multipliers, is

$$|g_n|^2 = \begin{cases} \tilde{\Gamma} - \frac{\Gamma_n}{\mathrm{SNR}[n]} & \tilde{\Gamma} - \frac{\Gamma_n}{\mathrm{SNR}[n]} \geq 0 \\ 0 & \tilde{\Gamma} - \frac{\Gamma_n}{\mathrm{SNR}[n]} < 0 \end{cases}$$

for a certain positive constant $\tilde{\Gamma}$.

A graphical representation of this solution, is called *water filling* or water pouring, which can be seen in Figure 4.2. The gains $|g_n|^2$ are put to "equalize" the SNR in each channel to get the constant $\tilde{\Gamma}$, the higher the SNR the higher the gain; some subcarriers with a low SNR may get $|g_n|^2 = 0$.

The overall bit rate becomes

$$R_\mathrm{b} = \frac{1}{T} \sum_{\substack{n=0 \\ g_n \neq 0}}^{N-1} \log_2 \left(\frac{\tilde{\Gamma}}{\Gamma_n} \mathrm{SNR}[n] \right)$$

which represents the maximum achievable bit rate for the specific channel, and there is no SNR margin

$$\lambda_n = 1 \qquad \forall n = 0, \ldots, N-1$$

4.2.2 Margin Maximization

As stated before, the total bit rate of the channel can be a fixed value. In this case, the allocation policy minimizes the total transmit energy

$$\min_{b_n} \left\{ \sum_{n=0}^{N-1} |g_n|^2 \right\}$$

with the bit rate constraint

$$\text{subject to} \quad \frac{1}{T} \sum_{n=0}^{N-1} b_n = R_\text{b}$$

The solution is again the water filling, but the energy is "poured" until we reach the desired bit rate R_b.

Margin Maximization with energy constraint

As the bit rate maximization solution, this solution has unit SNR margin for all subcarriers. If we assume a fixed transmit energy $\mathcal{E}$, we can multiply all the g_n by a factor of $\sqrt{\frac{\mathcal{E}}{\mathcal{E}_\text{min}}}$ where $\mathcal{E}_\text{min}$ is the total energy after the minimization

$$\mathcal{E}_\text{min} = \sum_{n=0}^{N-1} |g_n|^2$$

obtaining an SNR margin, equal among all subcarriers, of

$$\lambda_n = \frac{\mathcal{E}}{\mathcal{E}_\text{min}}$$

The SNR margin may be greater or lower than 1. If $\lambda_n > 1$ means that $\mathcal{E}_\text{min} < \mathcal{E}$ and the system can tolerate a decrease of SNR by a factor of λ_n maintaining the requirements, while $\gamma_n < 1$ means that the system cannot work with $\mathcal{E}$ and we have to increase the transmit energy to match at least $\mathcal{E}_\text{min}$

4.3 Practical allocation algorithms

The water filling algorithm provides the optimal solution to allocate bits and energies among subcarriers, but has two main drawbacks:

- Does not provide an efficient, hardware-implementable procedure.

- Assumes that b_n is a real number; it is usually defined a *granularity* β, which is the elementary increase of b_n, so that $b_n = m_n\beta$ for m_n integer. In most applications $\beta = 1$, *i.e.* b_n is an integer.

For these reasons, there are different algorithms to optimally allocate bits and gains with the granularity constraint. The two main algorithms are:

- Chow's algorithm [8]
- Levin-Campello algorithm [5, 20]

Chow's algorithm is a modification of the water filling procedure that takes into account β, while the Levin-Campello uses a different approach that achieves the same result.

In this work we adopted the Levin-Campello algorithm, described in the following section.

Levin-Campello algorithm

The Levin-Campello algorithm[1] achieves the optimal solution, both for the RA and MM problems, with a low complexity and an arbitrary value of β.

In the following explanation, we will show the algorithm that solves the Margin Maximization problem.

Introduction

The idea of the algorithm is recognizing that the overall performance of the system mainly depends on the highest BER; the algorithm tries to "level up" all subcarriers in order to have the same BER in all of them. Instead of allocating power like in water filling algorithms, this algorithm mainly allocates *bits*; this is to reduce the impact of nonlinearities in the system, which, especially for ADSL systems for which the Levin-Campello was originally designed, represent a major impact on system performance. The powers are allocated *after* the bit loading part to compensate for the granularity β.

Definitions

This algorithm distributes $b = R_\mathrm{b} \cdot NT$ bits among N subcarriers, each with signal-to-noise ratio SNR[n] for $n = 1, \ldots, N$. A function $r\mathrm{SNR}(b_n)$ (required SNR) is defined, depending on the target BER and the modulation/coding scheme, and is a function of the number of bits allocated in a subcarrier. All the signal-to-noise ratios, and the margins, are measured in *dB*.

There are two main variables in the algorithm: the current margin and the projected margin. The *current margin* λ_n is the difference (in decibels), between the measured SNR for the n-th subcarrier and the required SNR with b_n bits allocated

$$\lambda_n = \mathrm{SNR}[n] - r\mathrm{SNR}(b_n)$$

[1] Developed independently by Jorge Campello de Souza and Howard E. Levin

The *projected margin* $\mathcal{P}_n$ is the difference between the measured SNR and the required SNR with $b_n + \beta$ allocated bits, and represents the next margin in case another β bits are allocated in the n-th subcarrier

$$\mathcal{P}_n = \mathrm{SNR}[n] - r\mathrm{SNR}(b_n + \beta)$$

Bit allocation

At the beginning 0 bits are allocated amongst all subcarriers.

$$b_n = 0 \quad \forall n$$

Then the projected margin $\mathcal{P}_n$ is evaluated for all subcarriers, and we increment b_n on the subcarrier with the *highest* projected margin

$$b_n = b_n + \beta \qquad \text{with } n = \arg\max_m \{\mathcal{P}_m\}$$

The previous step is then repeated until all b bits are allocated.

Some subcarriers may have $b_n = 0$ because the SNR is too low, in this case the subcarrier is *shut down* and no signal is transmitted over it.

A pseudocode representation of the bit allocation part is shown in the following algorithm:

Algorithm 1 Bit allocation

```
for n = {0, ..., N − 1} do
    b_n ← 0
    P_n ← SNR[n] − rSNR(1)
end for
for k = {1, ..., N_bb} do
    n ← arg max_m{P_m}
    b_n ← b_n + β
    P_n ← SNR[n] − rSNR (b_n + β)
end for
```

Power allocation

The solution after the power allocation is not optimal due to the nonzero granularity β. This can be solved by allocating a gain vector g_n with the energy constraint

$$\sum_{n=0}^{N-1} |g_n|^2 = \mathcal{E}$$

At the beginning, the current margin γ_n is evaluated for all active subcarriers, and all the margins are summed to get the *geometric margin* γ

$$\gamma = \sum_{\substack{n=0 \\ b_n > 0}}^{N-1} \lambda_n$$

The unnormalized gains, in linear scale, are then calculated using

$$\mathfrak{g}_n = \begin{cases} 10^{(\gamma-\lambda_n)/20} & b_n > 0 \\ 0 & b_n = 0 \end{cases}$$

and then normalized to the target energy

$$g_n = \mathfrak{g}_n \sqrt{\frac{\mathcal{E}}{\sum_{n=0}^{N-1} |g_n|^2}}$$

A pseudocode representation of the power allocation and minimal margin part is shown in algorithm 1.

Minimal margin

At the end of the algorithm, a minimal margin $\lambda_{\min}$ is calculated with

$$\lambda_{\min} = \min_n \{20 \log_{10}(g_n) + \gamma_n\}$$

and represents the minimum margin that we get in the worst subcarrier. If this number is positive, the system is working and we can tolerate a maximum loss of $\lambda_{\min}$ dB SNR and have the system still working, while if this number is negative the system is not working and we have to change the requirements.

A pseudocode representation of the power loading is shown below, where the gains g_n and the margins λ_n are collected into $N \times 1$ vectors $\mathbf{g}$ and $\boldsymbol{\lambda}$.

Algorithm 2 Power loading and minimal margin calculation

```
1: γ = 0
2: for n = {1, ..., N} do
3:     if b_n > 0 then
4:         λ_n ← SNR_n − rSNR(b_n)
5:         γ ← γ + λ_n
6:     else
7:         λ_n ← ∞
8:     end if
9: end for
10: g ← 10^((γ−λ)/20)
11: g ← g · sqrt(E / g^† g)
12: λ_min ← min{20 log_10(g) + λ}
```

Chapter 5

System design

After reviewing the state-of-the-art of DMT-based optical communication systems in chapters 2, 3 and 4, in this chapter we will show the actual work done for this thesis, starting from the transceiver DSP design, followed by some detailed studies regarding specific issues that we encountered in the practical implementation of the system, and ending with the overall experimental setup.

5.1 Transceiver DSP

5.1.1 PAM vs DMT

In chapter 3, we described *two* modulation schemes suitable for self-coherent systems: PAM and DMT, and we anticipated that the choice for this work is DMT. We mainly choose DMT for its robustness against non-ideal channels, described in details in chapter 4, and its easy hardware implementation, due to the parallel processing and FDE.

An extensive comparison between PAM and DMT has been done by Fujitsu for the 100G Ethernet standardization process [21]; other comparisons can be found in [3, 16, 30].

5.1.2 Transmitter

The first thing we designed was the transmitter, its final scheme is shown in Figure 5.1. We are supposing that the bits do not come directly from a source but from a

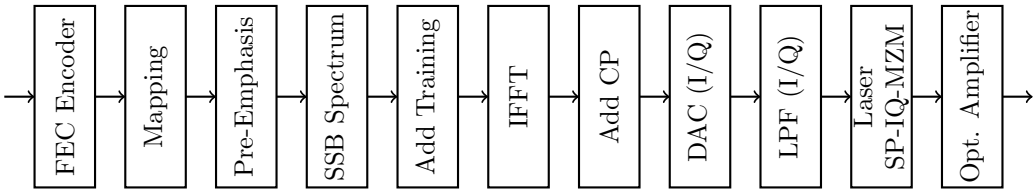

Figure 5.1: Block diagram of an optical DMT transmitter

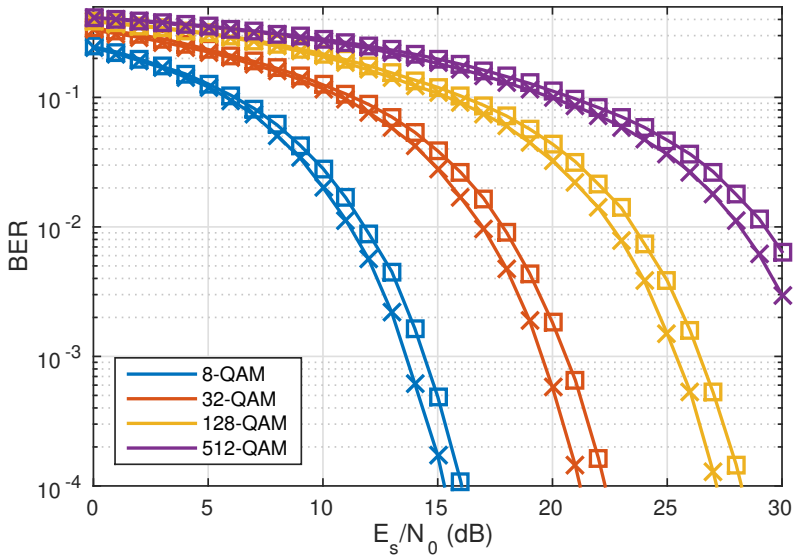

Figure 5.2: Comparison of rectangular (□) and cross shaped (×) constellations

FEC encoder, this is because the target BER of an optical communication system is below 10^{-14} and FEC is the only way to get this BER values for high-speed optical communications. FEC was not implemented in this work, therefore all the BERs shown are pre-FEC, and are compared to an FEC threshold, which in our work is 3.8×10^{-3}, that corresponds to the standard threshold for hard decision FEC in optical transport networks.

After the DMT modulation, the signal is sent to a DAC followed by a Lowpass Filter (LPF) which performs the operation in equation (3.8), and then is I/Q modulated and amplified using the techniques described in chapter 2.

Mapping

In this system we adopted modulation schemes with $n = 1, 2, \ldots, 10$ bits per symbol. For n even, we adopted standard QAM constellations, for $n = 1$ we used Binary Phase-Shift Keying (BPSK), while for n odd and greater than 1 there is not an optimal choice. The two possibilities we took into consideration are rectangular and cross QAM constellations. Rectangular-shaped constellations allow a Gray mapping but they are not very efficient in terms of average energy per symbol, while cross-shaped constellations do not have a Gray mapping but are more energy efficient.

A comparison of BER performance between these two shapes is shown in Figure 5.2, where we can see that cross-shaped constellations are slightly better ($\sim 1\,\text{dB}$ at $\text{BER} = 3.8 \times 10^{-3}$) than the rectangular shaped ones, therefore we choose to use cross-shaped constellations.

Pulse shaping

In a digital transmitter for optical communications, DACs bandwidth is one of the biggest limitations[1].

In optics, single-channel modulation formats are usually transmitted without any digital filtering, and the DAC low-pass effect is used to limit the bandwidth of the signal. In specific situations where the DAC output power is limited or the WDM grid is very strict, the signal is digitally upsampled and filtered with a low-pass filter (*e.g.* raised cosine) before being sent to the DAC. This increases the power efficiency and reduces the occupied optical bandwidth of the signal, but decreases the symbol rate.

In our specific system the DAC output power is limited and we cannot put a RF amplifier between the DAC and the modulator since the cost of a linear broadband amplifier will make the overall system unfeasible, therefore we decided to apply a digital filter before modulation. For multi-channel modulation, we achieved this effect by "switching off" some high frequency subcarriers, *i.e.* setting them to zero. This changes equations (3.10) and (3.12) as follows:

$$s[n] = \sqrt{\frac{1}{N_\mathrm{f}}} \sum_{k=0}^{N_\mathrm{f}-1} g_k S_\mathrm{ssb}[k] e^{j2\pi nk/N_\mathrm{f}}$$

$$S_\mathrm{ssb}[k] = \begin{cases} A[k] \in \mathcal{A}_k & k = 1, \ldots, N_\mathrm{m} \\ 0 & \text{otherwise} \end{cases}$$

Where the FFT size remains N_f and the number of modulated subcarriers reduces to $N_\mathrm{m} \leq N_\mathrm{f}/2 - 1$. If $N_\mathrm{m} = N_\mathrm{f}/2 - 1$ we get the same situation as equation (3.11), but if we decrease this number we can increase the sampling rate getting something equivalent to a digital pulse-shaping of the signal.

Skew compensation

A problem we encountered is the synchronization of the two DACs responsible to transmit the In-Phase and the Quadrature components of the signal. As we will show in section 5.2.4, even a small delay, called *skew*, between the two components (with respect to the DAC sampling rate) can degrade the performance. The DACs we employed allow us to tune the delay in integer multiples of the sampling rate, but cannot compensate for fractional delays.

First of all, we experimentally measured the delay by transmitting a BPSK signal at 36 GBd first in one DAC, switching off the other one, then we did the same of the other DAC. Using a sampling oscilloscope we measured the eye diagrams and we compared them to measure the time delay. Since the skew is caused by length differences between the RF paths, it is constant once the DACs are connected to the modulator. An example of eye diagram is shown in Figure 5.3, where the time delay is around 5 ps.

[1] For instance, the Fujitsu Leia DAC has a sampling rate of 65 Gs/s with a 3 dB bandwidth of 13 GHz

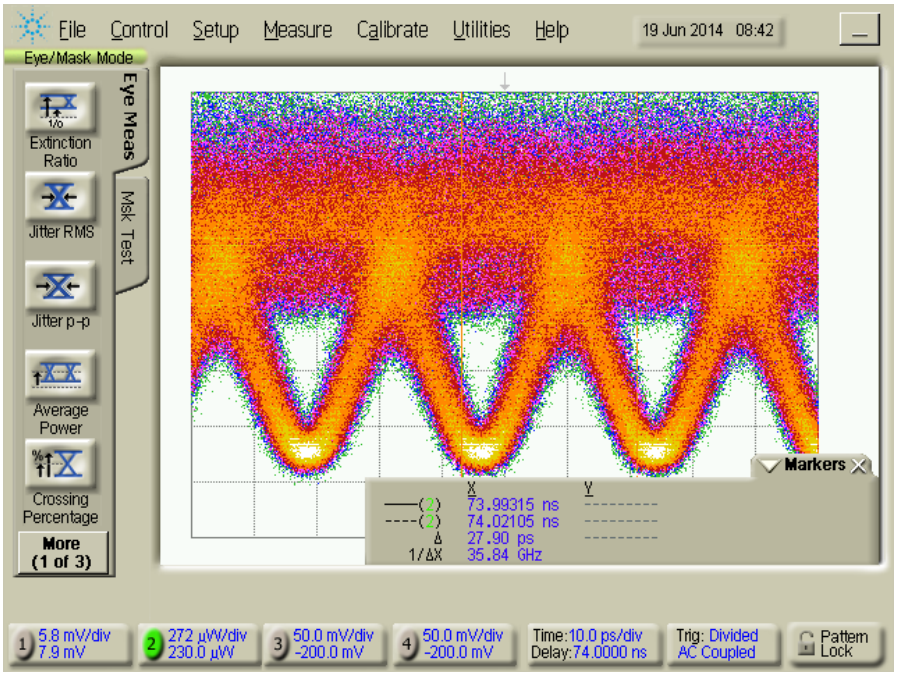

Figure 5.3: BPSK eye diagram for delay detection

After measuring it, we compensate it using a phase-only filter with frequency response

$$H_\tau[k] = \begin{cases} \cos(\pi\tau) & k = 0 \\ e^{j2\pi\tau(N_\mathrm{f}/2+1-k)/N_\mathrm{f}} & k = 1, \ldots, N_\mathrm{f}/2 - 1 \\ 1 & k = N_\mathrm{f}/2 \\ e^{-j2\pi\tau(-N_\mathrm{f}/2-1+k)/N_\mathrm{f}} & k = N_\mathrm{f}/2 + 1, \ldots, N_\mathrm{f} - 1 \end{cases}$$

where τ is the delay measured in samples.

Peak-to-average power ratio

A DAC is not a perfect linear device, but it has a limited output resolution (expressed in bits), which limits the output dynamic range. A b bit DAC has an output dynamic range which can be approximated as

$$20 \log_{10} 2^b \approx 6b \qquad \text{(dB)}$$

The effects of this limitation on the transmit signal depends on its PAPR γ^2, that is the ratio between the peak output and the average power of the signal

$$\gamma^2 = \frac{\max_t \left\{ |x(t)|^2 \right\}}{\left\langle |x(t)|^2 \right\rangle}$$

For M-PAM, the PAPR is

$$\gamma^2 = 3\frac{M-1}{M+1}$$

for instance, 4-PAM has a PAPR of 2.55 dB.

For DMT without power and bit loading the PAPR is [30]

$$\gamma^2 = 6(N-1)\frac{\sqrt{M}-1}{\sqrt{M}+1}$$

where M is the size of the M-QAM constellation and N the DMT block size. For instance, a 16-QAM constellation with a DMT block size of 512 samples has a PAPR of 32.64 dB, much greater than PAM. If this is not corrected in some way, the quantization noise of the DAC will heavily disrupt the quality of the communication.

To perform this, following [23], we note from equation (3.6) that a DMT signal is a sum of N independent random variables (assuming that the transmitted symbols are independent and identically distributed), and for $N \gtrsim 10$ for the central limit theorem we can assume the output signal to be Gaussian, with zero mean (assuming the DC tone is set to zero) and variance σ^2, which is also the power of the signal

$$p_{\text{DMT}}(x) = \frac{1}{\sqrt{2\pi}\sigma}e^{-x^2/(2\sigma^2)}$$

So, for instance, even if more than 99% of the amplitudes is contained between $\pm 3\sigma$, we can have a peak value of $\pm\gamma\sigma$, which in our example of 16-QAM $N = 512$ is approximately 42.64σ!

This means that we can *clip* the output with a negligible penalty but with a big benefit in terms of quantization noise added by the DAC. We say that a real signal $x(t)$ with power σ^2 and zero mean is clipped with clipping factor μ if we apply the following transformation

$$x_{\text{clip}}(t) = \begin{cases} x(t) & |x(t)| \leq \mu\sigma \\ \mu\sigma \cdot \operatorname{sgn}[x(t)] & |x(t)| > \mu\sigma \end{cases}$$

In this case, this adds a *clipping noise* to the signal with signal-to-clipping noise ratio

$$\text{SNR}_{\text{clip}} = \left[(1+\mu^2)\operatorname{erfc}\left(\frac{\mu}{\sqrt{2}}\right) - \sqrt{\frac{2}{\pi}}\mu e^{-\frac{\mu^2}{2}}\right]^{-1}$$

so by clipping the signal with a reasonable value, *e.g.* $\mu = 4$, we get an almost negligible clipping noise ($\text{SNR}_{\text{clip}} = 52.1$ dB) but we dramatically reduce the quantization noise introduced by the DAC.

5.1.3 Receiver

The overall structure of the DMT receiver is shown in Figure 5.4.

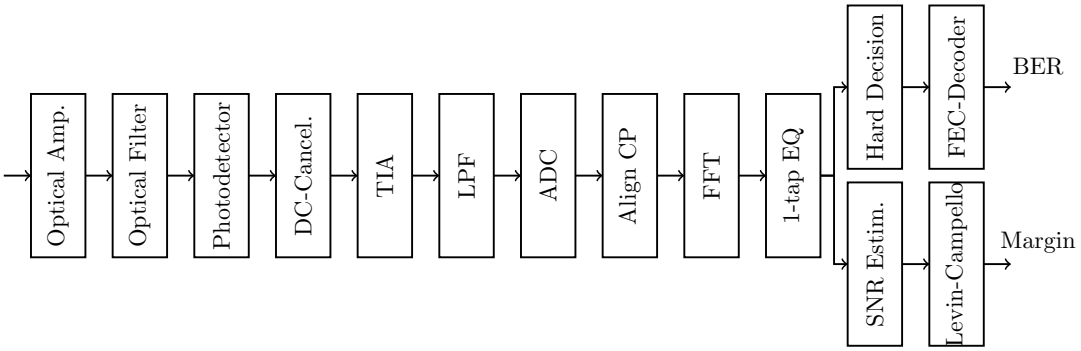

Figure 5.4: Block diagram of an optical DMT receiver

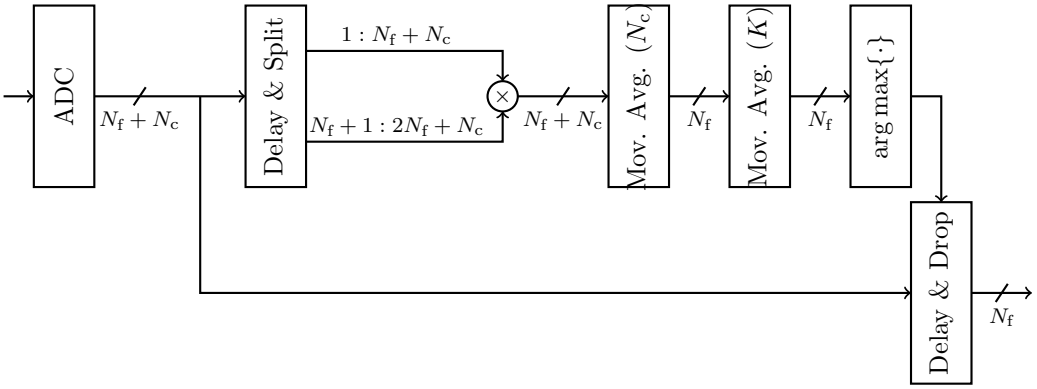

Figure 5.5: Cyclic prefix alignment

Cyclic prefix alignment

Before going to the frequency domain with the FFT, we have to detect and remove the cyclic prefix added by the transmitter, therefore we implemented the well-known Maximum Likelihood (ML) detection scheme [38] in a feed-forward structure, as opposed to the feedback structure, which is difficult to realize in hardware at the required speed. As opposed to [38], we did not estimate a frequency offset since we are demodulating the signal using the same carrier used to modulate it.

The main idea of the scheme is finding the maximum of the correlation of two sliding windows, each with length N_c, over an entire block with length N_f. To reduce noise, the correlation is averaged over K blocks with length $N_f + N_c$. The position of the cyclic prefix $\hat{n}$ can be therefore estimated with:

$$\hat{n} = \underset{0 \le n \le N_f - 1}{\arg\max} \left\{ \sum_{\ell=0}^{K-1} \sum_{m=0}^{N_c-1} y\left[n + m + \ell\left(N_f + N_c\right)\right] y\left[n + m + N_f + \ell\left(N_f + N_c\right)\right] \right\}$$

The block diagram of the scheme is shown in Figure 5.5. The received signal from the ADC is divided into blocks with size $N_f + N_c$. A delay and split component divides

the input data into two blocks, each with size $N_\mathrm{f} + N_\mathrm{c}$ but delayed by a factor of N_f, and multiplies them element-by-element. Then is run a moving average with length N_c inside each block and another moving average over K blocks, and the position of the maximum is the position of the cyclic prefix.

Equalization

After the FFT, we have to apply a FDE to the received subcarriers in order to perform hard decision. The equalizer coefficients $W[k]$ are not known *a priori* since we do not know the channel frequency response, but can be estimated using a sequence of training blocks N_te

$$W_0[k] = \sum_{\ell=0}^{N_\mathrm{te}-1} \frac{A_\ell[k]}{Y_\ell[k]}$$

and then updated using a decision-directed algorithm with a forgetting factor $d_\mathrm{e} < 1$

$$W_{m+1}[k] = (1 - d_\mathrm{e}) W_m[k] + d_\mathrm{e} \frac{\hat{A}_{m+N_\mathrm{te}}[k]}{Y_{m+N_\mathrm{te}}[k]}$$

Bitloading

Immediately after the equalizer there are two different paths where the signal can go:

- At the beginning the signal goes into a *calibration* path, where a (known) training sequence, which is QPSK on all subcarriers, is compared to the received signal, the SNR per subcarrier is calculated and the Levin-Campello algorithm, described in section 4.3, is applied.
- After calibration, the transmitter transmits different modulation formats on each subcarrier based on the Levin-Campello results, and the receiver compares the received bits with the transmit bits and calculates the BER.

In chapter 6, where the experimental results are shown, we will use both the minimal margin after Levin-Campello and the BER, based on the specific experimental conditions.

5.1.4 System parameters

After setting up the transceiver DSP using MATLAB, we run some simulations to debug the software and tune the main parameters in conditions similar to the experimental ones. The system parameters we chose are summarized in table 5.1.

5.2 Electrical and optical transmitter

5.2.1 Digital-to-Analog Converter

The analog signal is generated using two DACs at 72 Gs/s. These DACs, built with SiGe technology, have a high symbol rate maintaining a good bandwidth [33], and we have

Parameter	Description	Value	Unit
N_f	FFT size	512	samples
N_m	Modulated subcarriers	224	subcarriers
N_c	Cyclic prefix length	40	samples
OH_cp	Cyclic prefix overhead	7.25	%
f_s	DAC symbol rate	72	Gs/s
b_DAC	DAC resolution	6	bits
R_b	Gross bit rate	114	Gbit/s
M	Max bits per subcarrier	10	bits
N_bb	Bits per DMT block	874	bits
N_g	DMT blocks generated	512	blocks
μ	Clipping factor	4	-
tBER	Target BER	3.8×10^{-3}	-

Table 5.1: System parameters

used them in other experiments [32, 42]. They are controlled by an embedded Linux board, and we wrote some software to control it using MATLAB.

A low-speed DAC (MC DAC) applies the bias voltages to the MZM.

5.2.2 Carrier-to-signal power ratio

In the design of a self-coherent system, the most critical parameter is the CSPR, *i.e.* the ratio between the power of the carrier and the power of the signal. For this work we performed some calculations to find the best value.

Let us assume that the transmit signal is the sum of a zero-mean signal and the carrier

$$e_\mathrm{tx}(t) = ae(t) + c$$

where $e(t)$ has unit power, a and c are real positive constants with a total transmit power constraint

$$a^2 + c^2 = 1$$

Therefore the CSPR d^2 is

$$d^2 = \frac{c^2}{a^2}$$

The received signal, according to (2.2), is

$$y(t) = |ae(t) + c|^2 + n(t)$$

where $n(t)$ is an additive noise term that takes into account all noise contributions in the system (ASE noise, Johnson noise, ...).

After some algebra and the removal of the Direct Current (DC) term, we obtain

$$y(t) \propto 2\Re\{e(t)\} + \frac{1}{d}|e(t)|^2 + \frac{d^2+1}{d}n(t) \tag{5.1}$$

This equation tells us that a high CSPR reduces the SSBI, but at the same time will increase the input noise. As we will see in chapter 6, there is an optimal value of CSPR that represents the best trade-off between signal-signal beating and noise.

Signal-signal beating interference compensation

As shown in (5.1), the signal received with a photodiode is affected by SSBI, and its compensation is crucial to reach the goal of 100 Gbit/s. There are several compensation techniques described in literature, such as 2^{nd}-order Volterra equalizers [43] or iterative detection schemes [28], but all of them have a high computational complexity.

We therefore developed a novel scheme to reduce the impact of SSBI for a Single Side-Band signal with a low complexity. Assuming a transmit SSB optical field $e_{\text{ssb}}(t) = e(t) + j\,\mathcal{H}\{e(t)\}$, it gets impaired by CD with impulse response $h_{\text{cd}}(t)$ and detected using a photodiode according to (5.1). The received signal becomes

$$r(t) = [e(t) \otimes g_{\text{cd}}(t)] + \frac{1}{d}|e_{\text{ssb}}(t) \otimes h_{\text{cd}}(t)|^2 + \frac{d^2+1}{d} n(t)$$

where $g_{\text{cd}}(t)$ is a real signal whose Fourier transform is

$$G_{\text{cd}}(f) = \begin{cases} H_{\text{cd}}(f) & f > 0 \\ 0 & f = 0 \\ H^*_{\text{cd}}(-f) & f < 0 \end{cases}$$

The term inside the squared modulus can be expanded exploiting the fact that $e_{\text{ssb}}(t)$ is a SSB signal, and its convolution with the CD filter is a SSB signal as well

$$e_{\text{ssb}}(t) \otimes h_{\text{cd}}(t) = e(t) \otimes g_{\text{cd}}(t) + j\,\mathcal{H}\left\{e(t) \otimes g_{\text{cd}}(t)\right\}$$

and this is simply the SSB version of the signal-carrier beating.

Assuming a high signal-to-noise-and-distortion ratio the SSBI term can be well approximated with

$$\frac{1}{d}\,|e_{\text{ssb}}(t) \otimes h_{\text{cd}}(t)|^2 \approx \gamma\,|r(t) + j\,\mathcal{H}\{r(t)\}|^2$$

where $r(t)$ is the signal received by the photodiode defined in (2.4) and γ is a positive real-valued factor. According to this equation, we can compensate the SSBI by subtracting this term to $r(t)$, optimizing the value of γ.

In chapter 6 we will show some results with this scheme.

Bias method

When using scheme (B), we cannot directly set the CSPR since the only tunable parameter is ΔV, the difference between the bias applied to the modulator and the null. Nevertheless, there is a direct relation between ΔV and the CSPR which can be found using the MZM equation (2.3); its response centered around the null point is

$$e_{\text{out}}(t) \propto \sin\left(\frac{\pi}{2V_\pi^{(\text{rf})}} V_{\text{in}}(t) + \frac{\pi}{2V_\pi^{(\text{dc})}} \Delta V\right)$$

The combined power of the signal and the carrier is

$$P_{\mathrm{sc}} = P_{\mathrm{s}} + P_{\mathrm{c}} = \mathbb{E}\left\{\left|\sin\left(\frac{\pi}{2V_{\pi}^{(\mathrm{rf})}}V_{\mathrm{in}}(t) + \frac{\pi}{2V_{\pi}^{(\mathrm{dc})}}\Delta V\right)\right|^2\right\}$$

We assume that $V_{\mathrm{in}}(t)$ is a Gaussian process with zero mean and variance σ^2, while ΔV is deterministic.

If the signal is clipped between $-\mu\sigma$ and $\mu\sigma$ the variance is linked to the peak-to-peak voltage V_{pp} with the equation

$$\sigma^2 = \left(\frac{V_{\mathrm{pp}}}{2\mu}\right)^2$$

In this case, using the definition of expectation, the power becomes

$$P_{\mathrm{sc}} = \frac{1}{2} - \frac{1}{2}\exp\left[-2\left(\frac{\pi}{2V_{\pi}^{(\mathrm{rf})}}\right)^2\sigma^2\right]\cos\left(\frac{\pi}{V_{\pi}^{(\mathrm{dc})}}\Delta V\right)$$

The power of the carrier is

$$P_{\mathrm{c}} = \sin^2\left(\frac{\pi}{2V_{\pi}^{(\mathrm{dc})}}\Delta V\right)$$

and the carrier-to-signal power ratio is

$$\mathrm{CSPR} = \frac{1 - \exp\left[-2\left(\frac{\pi}{2V_{\pi}^{(\mathrm{rf})}}\right)^2\sigma^2\right]\cos\left(\frac{\pi}{V_{\pi}^{(\mathrm{dc})}}\Delta V\right)}{2\sin^2\left(\frac{\pi}{2V_{\pi}^{(\mathrm{dc})}}\Delta V\right)} \tag{5.2}$$

5.2.3 Bias control

Another important parameter to control is the bias point of the MZM, described in detail in section 2.3. This parameter is crucial to set the correct CSPR if using method (B), but also with method (C) it is important to bias the modulator at the null.

The main issue for finding the correct bias point of the modulator is that the point slowly changes with time, mainly due to changes in temperature. In commercial coherent systems there are devices called Automatic Bias Controllers (ABCs) which, using a low-speed feedback loop, are able to track the correct bias point. These devices cannot be used in our system since they are built for biasing at the null point and they use QPSK pilot tones, therefore we had to implement our own system.

Since the bias point is slowly changing with time, we manually bias the modulator before running any measurement. We tried to implement an automatic system but was not as effective as manual adjustment. The automatic system was kept to find an approximate solution, and then we manually adjusted the setting to the optimal value.

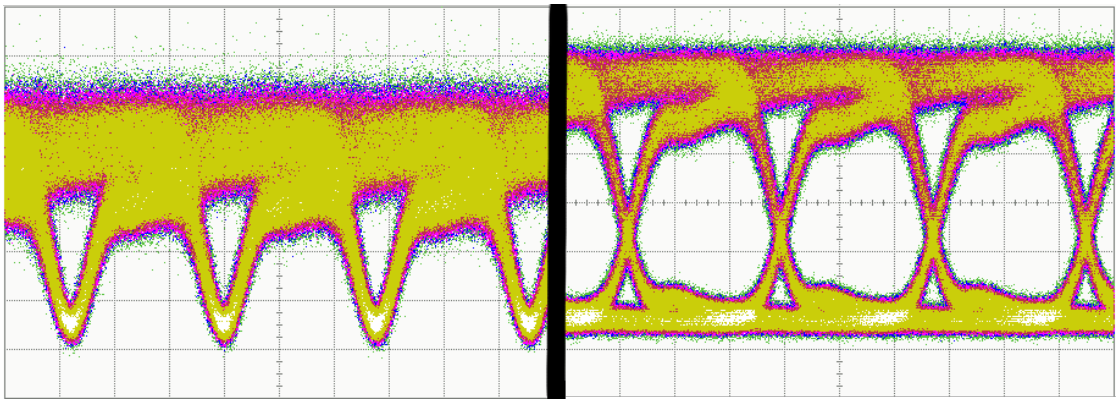

Figure 5.6: Left: BPSK at null. Right: BPSK at quadrature (NRZ-OOK)

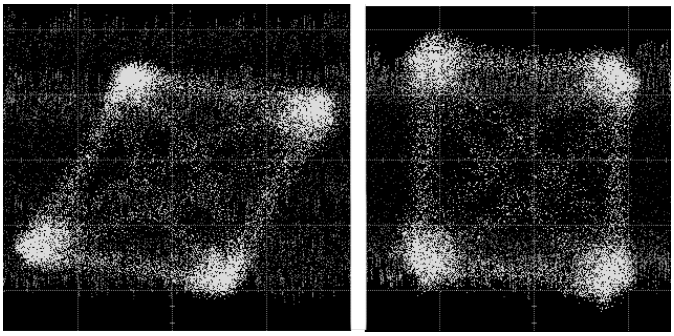

Figure 5.7: 18 GBd QPSK: wrong (left) and correct (right) common bias

To tune the I and the Q biases, we transmitted an 18 GBd BPSK signal, alternatively on both arms, and using the eye diagram to find the null. The null is the point in which the eye is at its maximum closure, as seen in Figure 5.6, left. As a comparison, in the same Figure on the right is represented the same signal biased at the maximum eye opening, which is the quadrature point, creating the so-called Non-Return-to-Zero (NRZ) On-Off Keying (OOK) modulation.

To tune the common (third) bias to $\pi/2$, we transmitted an 18 GBd QPSK signal and we connected a coherent receiver in homodyne configuration, *i.e.* the local oscillator is the transmit laser itself, in order to limit phase noise and avoid frequency offsets, and we looked at the received constellation in a 33 GHz, 80 Gs/s real time oscilloscope. If the angle is not $\pi/2$ the received constellation is a parallelogram, while when the angle is exactly $\pi/2$ we get a square. An example of this measurement is shown in Figure 5.7.

5.2.4 Effect of I/Q imbalance on SSB

In an SSB-DMT system, the performance of the receiver is very sensitive to transmitter imbalances between the I and the Q components. For instance, the coaxial cables that connect the DACs to the modulator can be slightly different, which can introduce a delay τ between these two components, and the modulator does not shift these two component by exactly $\pi/2$ radians, but there can be an error θ in the phase shift.

To analyze this, let us analyze the real and the imaginary parts of the Fourier transform of the SSB optical field $E_{\text{ssb}}(f) = E^{\text{r}}_{\text{ssb}}(f) + jE^{\text{i}}_{\text{ssb}}(f)$. Both of them are real in time domain, so in frequency domain they express Hermitian symmetry. In addition, $E_{\text{ssb}}(f)$ has no negative frequency components. To express these conditions, we introduce a placeholder function $Q(f)$ which is the positive spectrum of $E_{\text{ssb}}(f)$

$$E_{\text{ssb}}(f) \triangleq \begin{cases} Q(f) & f \geq 0 \\ 0 & \text{otherwise} \end{cases}$$

Using this definition, the real and imaginary parts are

$$E^{\text{r}}_{\text{ssb}}(f) = \begin{cases} \frac{1}{2}Q(f) & f \geq 0 \\ \frac{1}{2}Q^*(-f) & f < 0 \end{cases}$$
$$E^{\text{i}}_{\text{ssb}}(f) = \begin{cases} \frac{1}{2j}Q(f) & f \geq 0 \\ -\frac{1}{2j}Q^*(-f) & f < 0 \end{cases}$$

We can now start applying the time delay and phase shift between the real and imaginary part. The transmitted SSB signal is therefore

$$E_{\text{ssb}}(f) = E^{\text{r}}_{\text{ssb}}(f)e^{+j(\theta+2\pi\tau f)/2} + jE^{\text{i}}_{\text{ssb}}(f)e^{-j(\theta+2\pi\tau f)/2}$$

Using the definition of $Q(f)$ we get

$$E_{\text{ssb}}(f) = \begin{cases} \frac{1}{2}Q(f)\left[e^{+j(\theta+2\pi\tau f)/2} + e^{-j(\theta+2\pi\tau f)/2}\right] & f \geq 0 \\ \frac{1}{2}Q^*(-f)\left[e^{+j(\theta+2\pi\tau f)/2} - e^{-j(\theta+2\pi\tau f)/2}\right] & f < 0 \end{cases} =$$
$$= \begin{cases} Q(f)\cos\left[(\theta + 2\pi\tau f)/2\right] & f \geq 0 \\ Q^*(-f)j\sin\left[(\theta + 2\pi\tau f)/2\right] & f < 0 \end{cases}$$

and the flipped conjugate version of this signal is

$$E^*_{\text{ssb}}(-f) = \begin{cases} -Q(f)j\sin\left[(\theta - 2\pi\tau f)/2\right] & f > 0 \\ Q^*(-f)\cos\left[(\theta - 2\pi\tau f)/2\right] & f \leq 0 \end{cases}$$

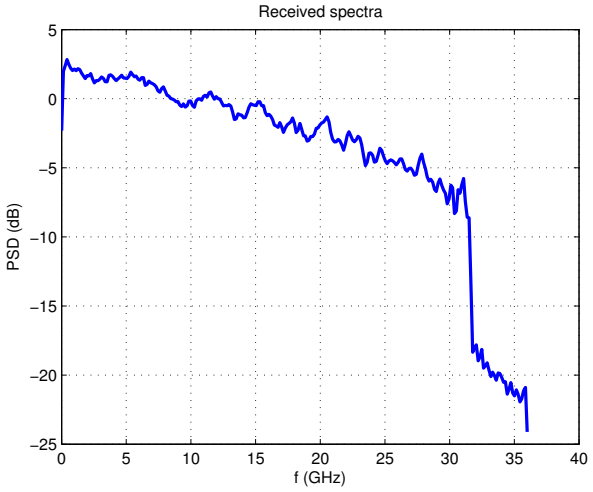

Figure 5.8: DMT over 80 km SSMF with $\tau \approx 0$

By transmitting over a distance d of optical fiber and receiving it using a self-coherent system, according to (2.4), we get

$$SC(f) = \begin{cases} Q(f)\left[\cos\left(\frac{\theta+2\pi\tau f}{2}\right)e^{-j\left(\beta_2 f^2 d/2\right)} - j\sin\left(\frac{\theta-2\pi\tau f}{2}\right)e^{+j\left(\beta_2 f^2 d/2\right)}\right] & f \geq 0 \\ Q^*(-f)\left[j\sin\left(\frac{\theta+2\pi\tau f}{2}\right)e^{-j\left(\beta_2 f^2 d/2\right)} + \cos\left(\frac{\theta-2\pi\tau f}{2}\right)e^{+j\left(\beta_2 f^2 d/2\right)}\right] & f < 0 \end{cases} =$$
$$= E(f)H_{\theta,\tau}(f)$$

which means that we get the original Dual SideBand (DSB) signal,

$$E(f) = \begin{cases} Q(f) & f \geq 0 \\ Q^*(-f) & f < 0 \end{cases}$$

impaired by a linear filter $H_{\theta,\tau}(f)$ which is not anymore all-pass but is frequency-selective, and this will reduce the performance of the system.

For instance, let us compare the performance of a 72 Gs/s DMT system over 80 km of SSMF without any delay and with a delay $\tau \approx 5\,\text{ps} = 0.36T$. As we can see, the delay creates notches in the spectrum which reduce the overall system performance.

5.2.5 Experimental setup

After solving the aforementioned problems, we started building the actual transmitter for the experiment.

We started from the laser, which was a standard telecom External Cavity Laser (ECL), set at frequency $f_0 = 193.1$ THz (or wavelength $\lambda_0 = 1552.52$ nm). Then we connected the DACs to the $LiNbO_3$ MZM using two 10 cm coaxial cables and the low-speed MC DAC to the biases of the modulator.

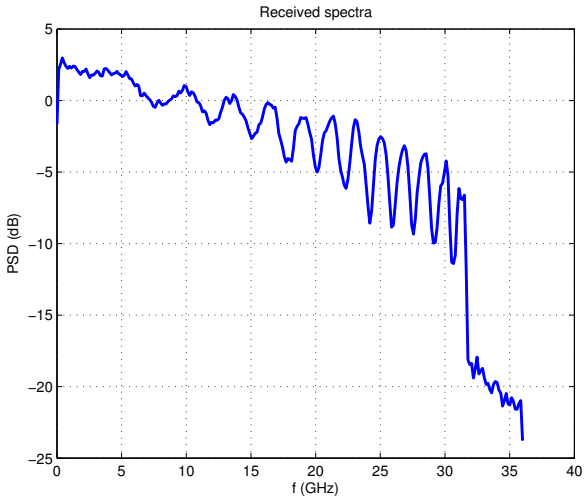

Figure 5.9: DMT over 80 km SSMF with $\tau \approx 5$ ps

Parameter	Description	Value	Unit
$V_\pi^{(\mathrm{dc})}$	MZM drive voltage at DC	8.5	V
$V_\pi^{(\mathrm{rf})}$	MZM drive voltage at RF	3	V
B_o	MZM optical bandwidth	22	GHz
P_l	Laser output power	15.5	dBm
f_0	Laser frequency	193.1	THz
λ_0	Laser wavelength	1552.52	nm

Table 5.2: Transmitter parameters

After that, we implemented the two transmitter structures Ⓑ and Ⓒ described in section 2.4.2. The transmitter parameters used for the experiment are summarized in table 5.2.

Bias method For this case we just connected directly the modulator after the laser, and we tuned the bias using a software we wrote for the low-speed DAC. On Figure 5.10 is shown a picture of the transmitter setup.

External carrier path In the experiment we also tried scheme Ⓒ of Figure 5.11, where the carrier is added using an external (with respect to the modulator) path. A picture of the setup is shown on Figure 5.12.

In this scheme a 90/10 tap is put immediately after the laser, and while in one arm we put the modulator, in the other we put a VOA to tune the CSPR. After that, a 3 dB tap combines together the carrier and the signal. Since the self-coherent system works

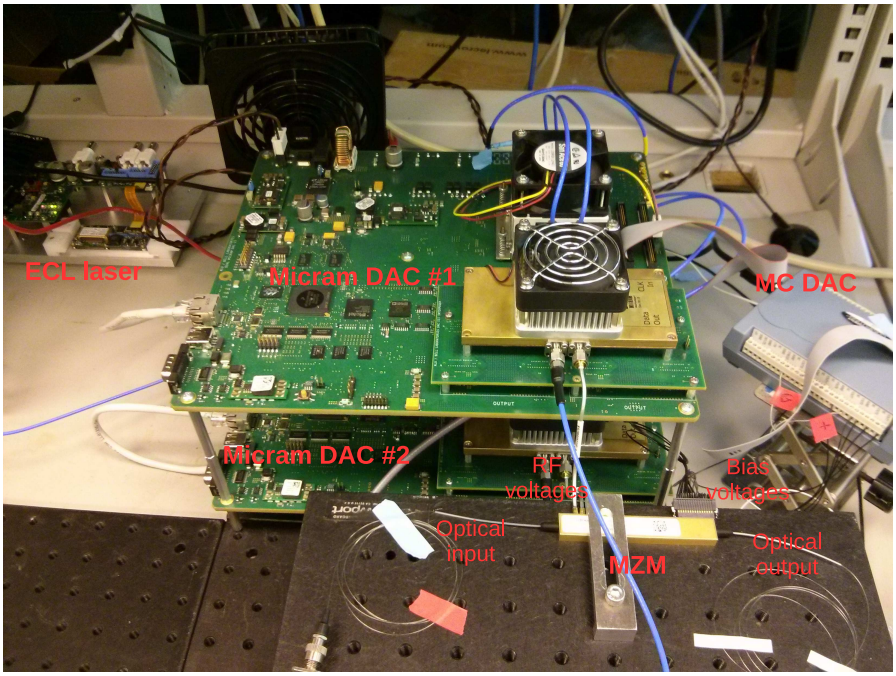

Figure 5.10: Transmitter picture

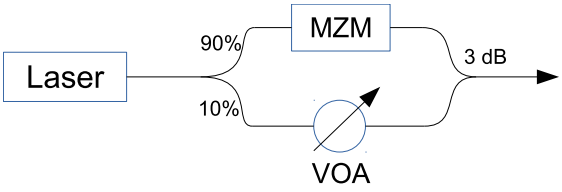

Figure 5.11: External carrier path scheme

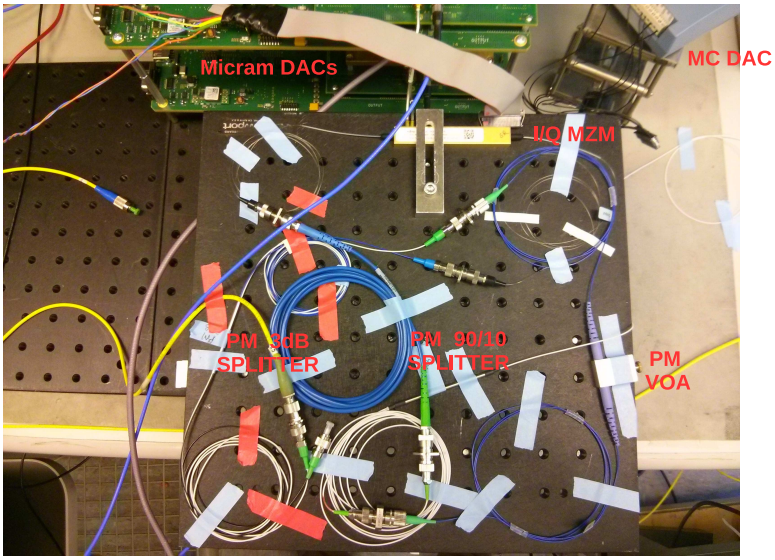

Figure 5.12: External carrier path picture

Parameter	Description	Value	Unit
CG	TIA conversion gain	200	V/W
R	Photodiode DC responsivity	0.585	A/W
$f_{3\,\mathrm{dB}}$	3 dB cutoff frequency	40	GHz
i_{noise}	Equivalent input noise density	40	$\mathrm{pA}/\sqrt{\mathrm{Hz}}$
f_{s}	ADC sampling rate	160	Gs/s
b_{ADC}	ADC resolution	8	bits

Table 5.3: Receiver parameters

only if the signal and the carrier are on the same polarization, all the optical components are Polarization Maintaining (PM), increasing the cost of the system.

5.3 Electrical and optical receiver

As photodetector, we first used a regular PiN photodetector, but the sensitivity was too low and it was required a very high received power (around +7/+8 dBm). Then we decided to employ a PiN photodiode followed by a low-noise Transimpedance Amplifier (TIA), and this decreased the optimal received power. The results of this experiment are shown in details in the chapter 6. The main receiver parameters are summarized in table 5.3. The photodetector is connected to a real time oscilloscope that digitizes the output of the photodiode, and saves in its memory the captured waveform. The waveform is then offline processed using a computer with the algorithms described in section 5.1.3; the photodetector and the scope are shown in Figure 5.13.

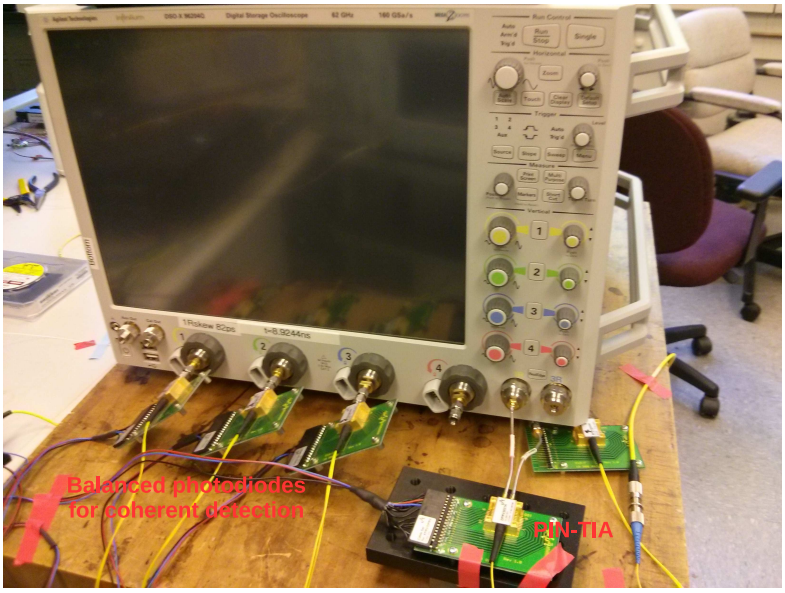

Figure 5.13: PiN-TIA and oscilloscope

Since in our experiment we did not implement a timing recovery scheme, we connected a BNC cable from the clock generator that drives the DACs to the real time oscilloscope to deliver a 10 MHz reference clock that synchronizes the sampling instants.

5.4 Transmission

After building the transmitter and the receiver, we started building the whole communication system. We first started connecting the transmitter directly to the receiver, called *back-to-back* configuration, and then we connected spools of fiber in between to build the final system

Amplification

Due to the Gaussian distribution of the amplitude of a DMT signal, as described in section 5.1.2, the modulation has a high insertion loss, so we decided to put a booster amplifier immediately after the transmitter. We put another amplifier immediately before the receiver in order to recover the signal power dissipated during transmission.

To keep the system cost-effective, we employed *mini EDFAs*, which are smaller and cheaper than regular EDFAs, but with a worse noise figure and low output power. The EDFA parameters are reported in table 5.4.

At the receiver we also tried an SOA, with parameters written in table 5.5. A SOA has a worse noise figure and high nonlinearities, like XGM, but it is more appealing since it can be easily integrated in the optical transceivers.

Parameter	Description	Value	Unit
P_{max}	Maximum output power	17.5	dBm
G_{n}	Nominal gain	23	dB
F_{n}	Average noise figure	5	dB

Table 5.4: EDFA parameters

Parameter	Description	Value	Unit
G_{max}	Maximum gain	27.3	dB
F_{n}	Average noise figure	6.4	dB
P_{sat}	Saturation power (3 dB)	13.6	dBm

Table 5.5: SOA parameters

Setup

To test this configuration and to emulate the attenuation of transmission over fiber, a VOA is put between the transmit and receive amplifiers. For transmission two spools of 20 km and 60 km of SSMF are used. The amplifiers with the VOA and the fiber spools are shown in figures 5.14 and 5.15.

At the receiver, especially after transmission over a long distance, the signal is corrupted by ASE noise. Since the receiver is non-coherent, it is important to remove noise outside the signal bandwidth, and for this reason we put a broadband optical filter with bandwidth 175 GHz immediately after the receiver amplifier. After the optical filter, a 90/10 tap sends 10% of the light to the Optical Spectrum Analyzer (OSA) for monitoring, then the 90% arm is connected to the photodetector; this setup is shown in Figure 5.16. The OSA is an important diagnostic tool that we used to verify and debug the setup. The overall system is shown in Figure 5.17.

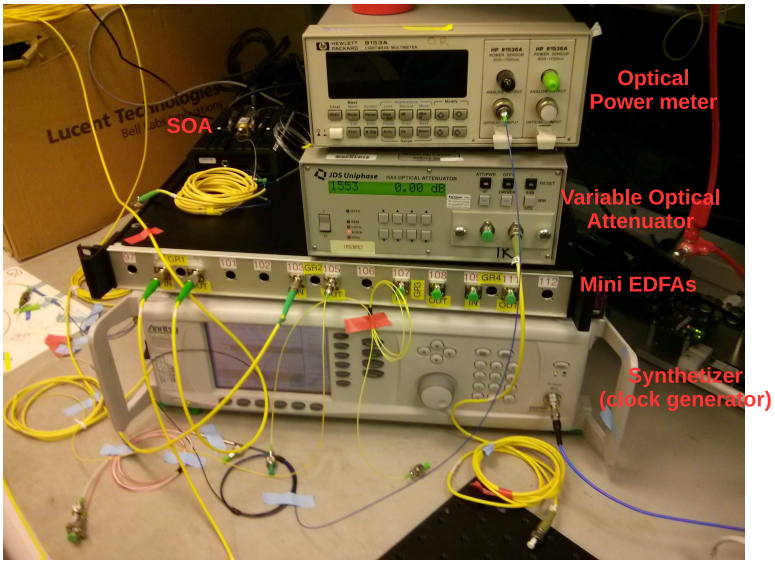

Figure 5.14: Amplifiers and VOA

Figure 5.15: Spools of SSMF

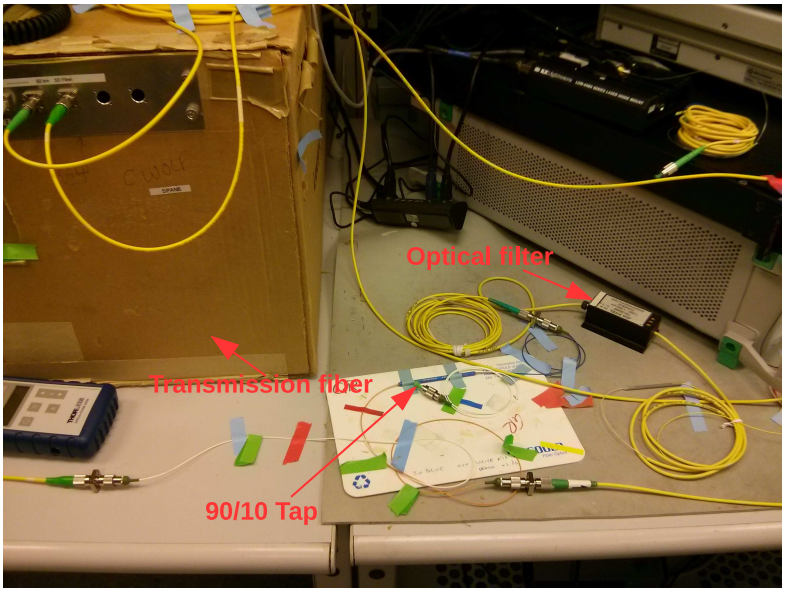

Figure 5.16: 90/10 tap and optical filter

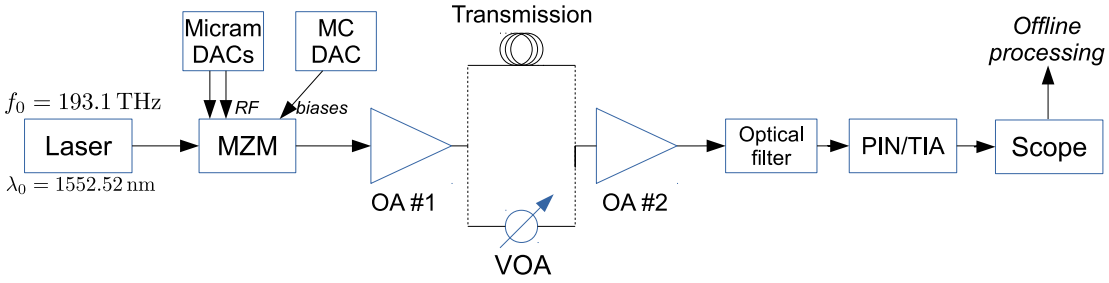

Figure 5.17: Overall experimental setup

Chapter 6

Experimental results

6.1 Introduction

In this chapter we will present the experimental results measured with the setup described in chapter 5.

As a performance indicator, we will use either the *minimal SNR margin* or the *average BER*. For the BER measurements, we applied the Levin-Campello algorithm to the SNR measured in the optical back-to-back experiment with no attenuation, while for the SNR measurements we used the system in the calibration mode, transmitting QPSK in all the subcarriers. As stated in the introduction, the bit and power mapping are *static* since the absence of a feedback channel is a requirement of the system.

The BER has been used for the main transmission experiments (like the back-to-back curve or the power sweeps during transmission), while the SNR has been used in the sweeps to find the best system parameters.

6.2 Back-to-back

In this section we disconnected the fiber spools and connected the VOA. If there is no attenuation value specified, is implicit that the attenuation is 0 dB.

6.2.1 Calibration

Carrier-to-signal power ratio The first parameter we have to tune is the CSPR. As shown in (5.1), there's an optimal trade-off between the carrier and the signal power, this can be clearly seen in Figure 6.1. The Figure compares the two mechanisms that we experimentally used to add the carrier, the bias point method Ⓑ, and the external carrier path method Ⓒ, defined in section 2.4.2. The optimal CSPR is approximately the same, but the bias point method has a better performance of 0.6 dB due to a better control of the carrier phase.

In scheme Ⓒ, the CSPR has been measured by looking at the signal power after switching out the carrier path and the combined signal+carrier power. The results are

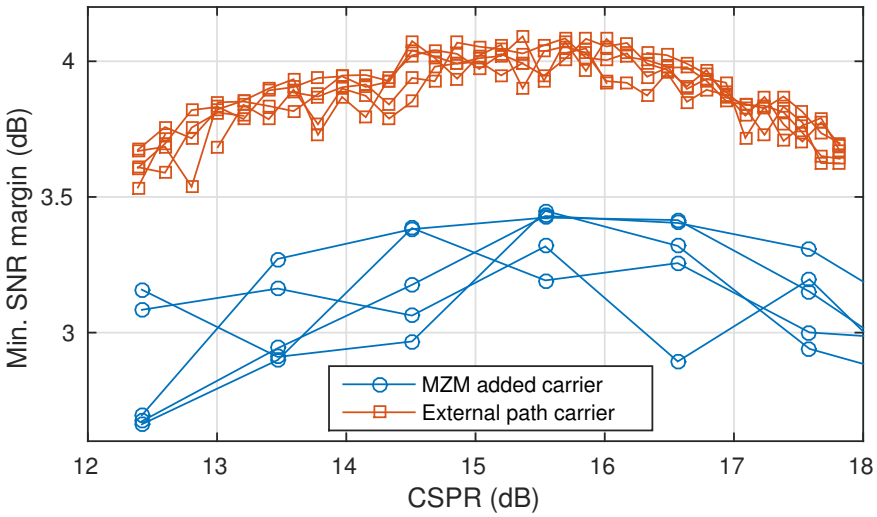

Figure 6.1: CSPR in back-to-back, 5 waveforms

more "noisy" due to the manual adjustment of the VOA. In scheme (B), the CSPR is estimated from the voltage difference ΔV from the null applied to the modulator, using (5.2).

In the next experiments we will use this optimal CSPR value.

SSBI compensation In chapter 5, we shown our proposed SSBI compensation scheme. To test the scheme, we took the same data we measured for Figure 6.1 with scheme (B) and we run the receiver DSP without any SSBI compensation. The results are shown in Figure 6.2, together with the original data. We can see a significant improvement in SNR margin to as much as 4 dB, and a shift of the optimal CSPR value. This fact can be understood from (5.1), since a high CSPR reduces the impact of SSBI but increases the noise.

Photodetectors As stated in section 5.3, we compared a PiN photodiode with an integrated PiN-TIA. The difference between these two different receivers is shown on Figure 6.3.

We measured the SNR margin as a function of the photodiode input power, set using a VOA immediately before it. In this case, we can see that the PiN-TIA has a greater sensitivity (around 8 dB) than the regular PiN photodiode, and can achieve better performance due to the limited output power of the EDFA. Increasing the input power increases the performance until a maximum is reached, then the photodiode saturates and the performance slightly decreases.

Additionally, we measured the PiN-TIA curve with a fixed attenuation of 17 dB between the amplifiers, which is the nominal attenuation of 80 km of SSMF. The presence

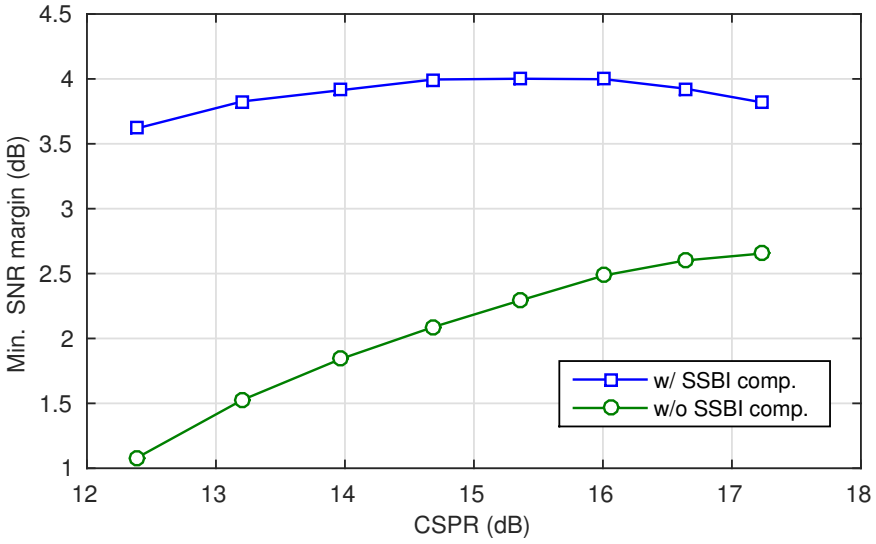

Figure 6.2: CSPR with and without SSBI compensation

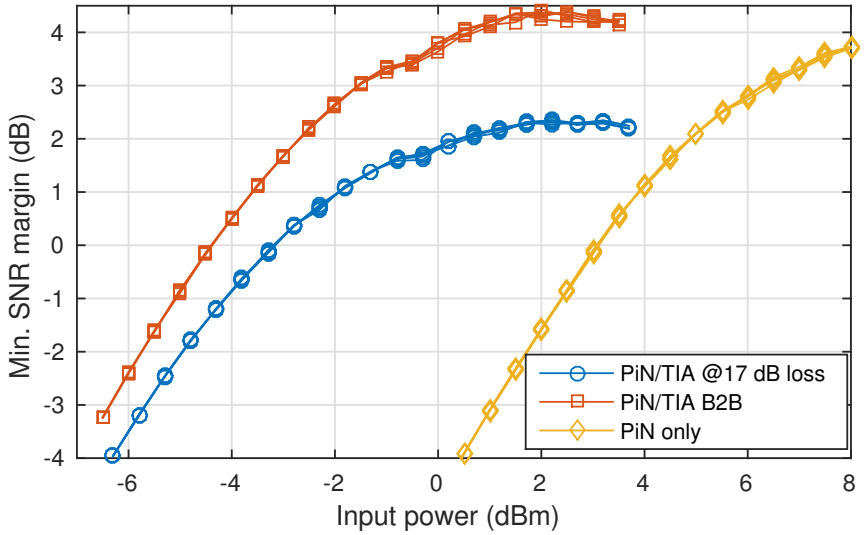

Figure 6.3: Photodiodes response

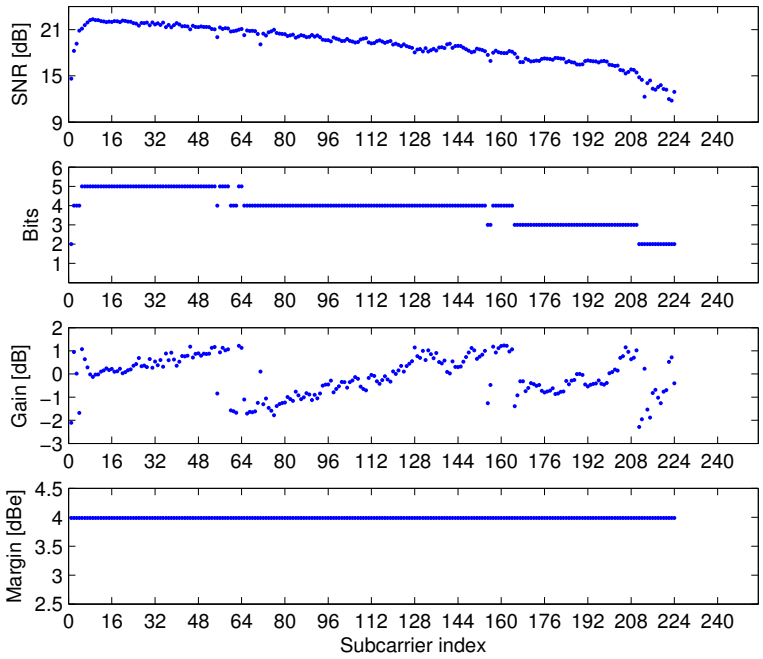

Figure 6.4: Levin-Campello results

of ASE noise reduces the overall performance but keeps the best input power at the same level, between 1 and 2 dBm.

In the next experiments, we will use the optimal input power of 1.5 dBm.

Levin-Campello After the calibration of the experiment parameters, we accurately measured the SNR in every subcarrier and applied the Levin-Campello algorithm to generate an optimal bit and power allocation that will be used in all future bit transmission experiments. The results are shown in Figure 6.4.

We can see that the channel has a lowpass charateristic, but few subcarriers close to the carrier are worse due to the impact of signal-signal beating (5.1). The Levin-Campello employs a range of modulation formats from QPSK to 32-QAM, achieving a minimum SNR margin of 4 dB.

6.2.2 Experiment

Attenuation/BER curve After the Levin-Campello, we measured how the BER scales with the attenuation between amplifiers to see how our system scales with distance. The results are shown in Figure 6.5.

From the results we see that after a floor around 2×10^{-5}, the BER increases linearly (in log-log scale) with attenuation, reaching the BER threshold at 20.7 dB of attenuation,

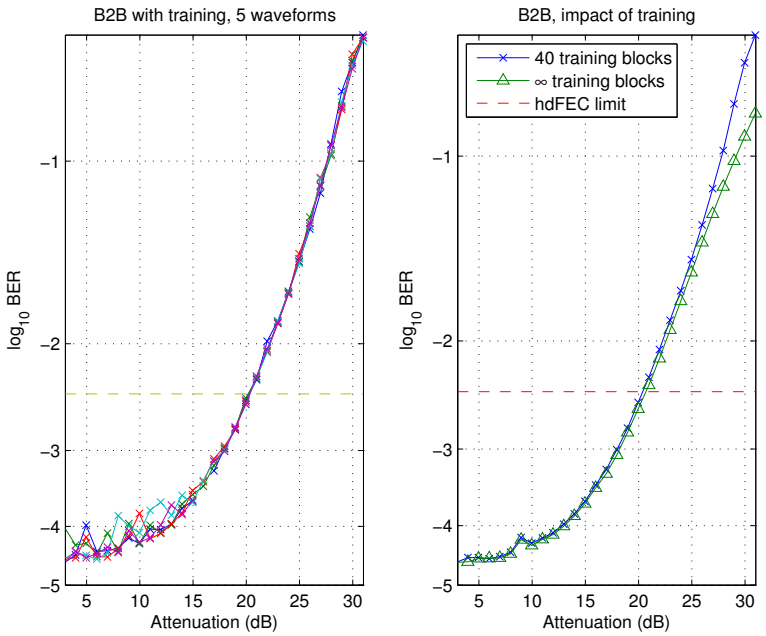

Figure 6.5: Attenuation vs BER curve

which corresponds to 103.5 km of SSMF. In this case, we can say that the goal of 80 km transmission can be reached.

In the plot on the right we compare the performance of the equalizer in full training mode and in training plus tracking mode with a limited number of training blocks. We can see that for BERs lower than the threshold the difference is negligible, while for higher BERs the difference becomes bigger.

Guard band In the previous section, we showed the average BER among all subcarriers, which is the relevant value in case of jointly coded subcarriers. Showing instead the single BER among all subcarriers, we can see that the maximum BER can be higher than the average BER. This is mainly caused by the first subcarriers, close to the carrier, since are mainly affected by nonlinearities and their SNR measurement is not accurate.

To try to solve this problem, we tried to shut down some subcarriers, creating a "guard band" between the carrier and the signal. From the results in Figure 6.6, we can see that by shutting down few subcarriers, 2 or 3 at most, the average BER stays the same, but the difference between maximum and average BER decrease dramatically, increasing the system reliability. Greater guard band length doesn't improve the difference but slightly decreases the performance due to the lowpass effect of the channel.

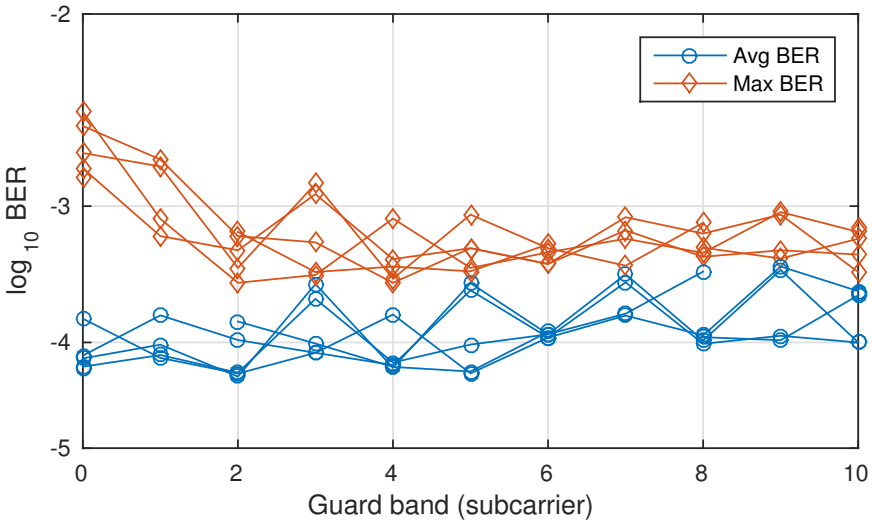

Figure 6.6: Guard band results

6.3 Transmission

In the next sections we will show transmission experiments over 20, 60 and 80 km of SSMF.

6.3.1 Calibration

Carrier-to-signal power ratio At first we run another carrier-to-signal power ratio sweep using the same method employed for the back-to-back measurement. The results, shown in Figure 6.7, show that there is an optimal value, but it is lower than the back-to-back measurements. This is mainly due to fiber nonlinearities, not present in back-to-back.

In the next transmission experiments, instead of using this maximum, we adopted the optimal value in back-to-back, since the Levin-Campello results is tied to a specific CSPR.

6.3.2 Experiment

Launch power We then measured different launch power at the booster amplifier for the three adopted transmission distances, shown on Figure 6.8.

We can see that an increase of the launch power corresponds to an increase in optical SNR and an increase in performance, until the fiber nonlinearities (mainly Stimulated Brillouin Scattering (SBS)) are triggered, starting from 10 dBm, that generate power fluctuation in the received waveform.

We then see that the optimal transmit power is 9 dBm, and using this power we are able to transmit under the BER threshold at all the distances.

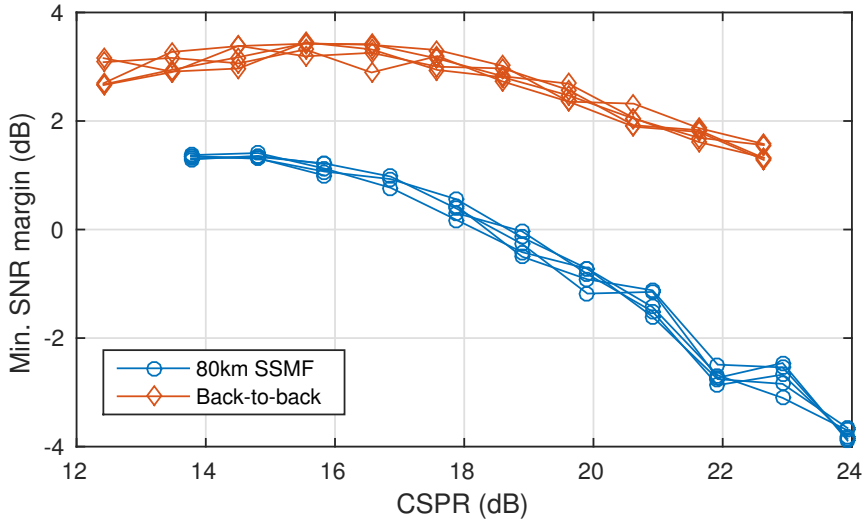

Figure 6.7: CSPR sweep at 80 km

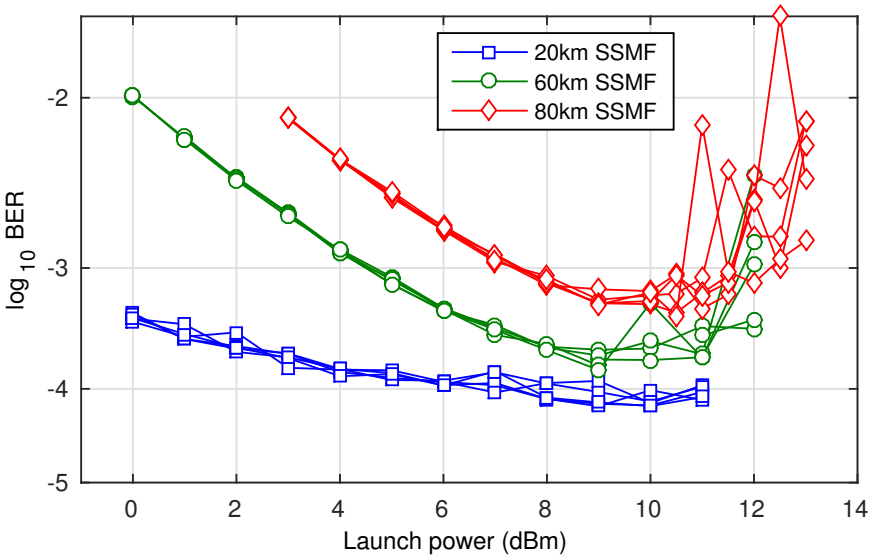

Figure 6.8: Launch power at different distances

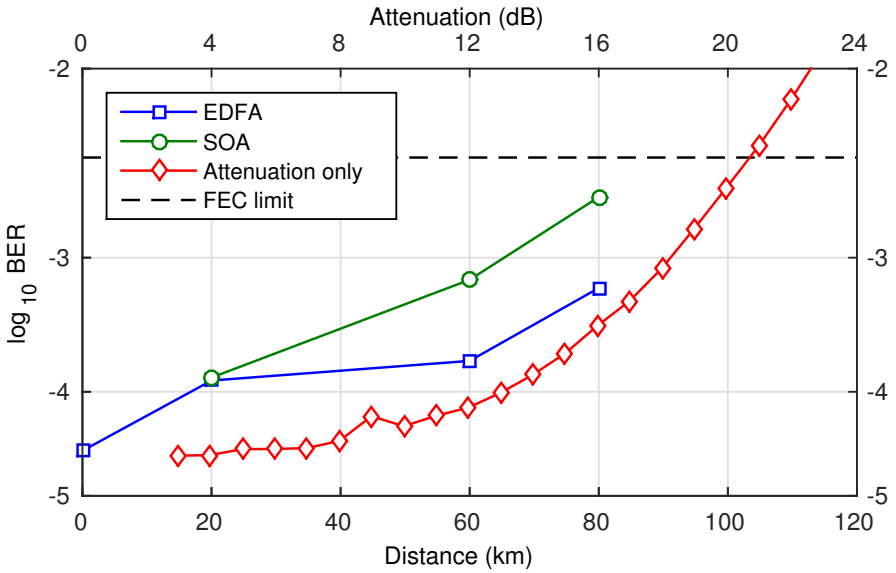

Figure 6.9: BER with with distance using EDFAs and SOA

Semiconductor Optical Amplifiers We then employed an SOA as a receiver amplifier; the results are shown in figure 6.9.

The results of the back-to-back curve and transmission using two EDFAs and one EDFA+SOA are compared. We can see that there is a transmission penalty compared to the back-to-back, as expected, and the SOA decreases the overall performance, but at 80 km the system is still under the FEC threshold.

Chapter 7

Conclusions

In this work we have designed and implemented a complete optical communication system, with a maximum raw bit rate of 114 Gbit/s over distances up to 80 km.

We first started analyzing the most common transmitter and receiver structures adopted in optical communications, focusing on the self-coherent structure, in which we transmit a carrier along with a real-valued signal that can be received with a single photodetector, without the need of a coherent receiver and simplifying the Digital Signal Processing (DSP) algorithms. For these systems chromatic dispersion is one of the main impairments, and we presented Single Side-Band (SSB) as a method to compensate it, with a slight increase in transmitter complexity. SSB also provides an increase in spectral efficiency.

We then focused on the digital modulation schemes that can be adopted in self-coherent systems, focusing on the multi-carrier Discrete Multitone (DMT) scheme, which allows to divide the bandwidth of the channel into several sub-channels and allocate a different bit rate based on the quality of each sub-channel. The optimal allocation method is based on the calculation of channel capacity for DMT channels, and we presented the Levin-Campello algorithm to achieve this.

We then started designing the system, starting from the DMT transceivers. We built a model to study the impact of transmitter impairments on the received signal, and we developed a novel Signal-Signal Beating Interference (SSBI) compensation scheme that allowed us to reduce the Bit Error Rate (BER) and the Carrier-to-Signal Power Ratio (CSPR). After that, we built an experimental setup to measure the performances of the system we designed, measuring the Signal-to-Noise Ratio (SNR) and the BER at different distances and noise levels.

At the beginning we calibrated the system, finding the optimal values of the system parameters, and we run the Levin-Campello algorithm to obtain the best bit allocation among the subcarriers. We then measured the BER in back-to-back with Amplified Spontaneous Emission (ASE) noise loading and after transmission over different spans of Standard Single-Mode optical Fiber (SSMF). In the experiment we transmitted a raw bit rate of 114 Gbit/s, which takes into account a 12% Forward Error Correction (FEC) overhead and an additional 2% overhead for training symbols.

From the results, we saw that the BER is below the hard FEC threshold both in back-to-back (Figure 6.5) and in transmission (Figure 6.9), which means that DMT with SSB is a feasible option for 100G transmission over 80 km, using SSMF over C-band, using both Erbium Doped Fiber Amplifier (EDFA) and Semiconductor Optical Amplifier (SOA) amplification. Nevertheless, there are still problems that have to be tackled. For instance, the system is very sensible to the amplitude and phase of the carrier added at the transmitter. In the experiment we compared the carrier added by Mach-Zehnder Modulator (MZM) with a custom bias point and an interferometric structure (Figure 6.1), and we found the MZM to be more effective since, being an integrated optical circuit, it has greater control of the phase in the arms. The MZM solution is not easy to implement in a commercial system, since there are no Automatic Bias Controllers (ABCs) able to track a custom bias point, therefore it is necessary to build a custom integrated modulator. Additionally, we used very ideal (and expensive) components, especially the Digital-to-Analog Converters (DACs) and the oscilloscope, which cannot be used in a commercial low-cost implementation.

These problems have to be solved in future works in order to develop a commercial implementation.

Appendix A

Conventions

A.1 Notation

In this work we will use the following notation:

Numbers are complex unless explicitly stated differently, with $j = \sqrt{-1}$

Scalars are written as lowercase italic characters, *e.g.* a

Vectors are, unless explicitly indicated, column vectors and are lowercase bold-faced characters, *e.g.* $\mathbf{a}$

Matrices are uppercase bold-faced, *e.g.* $\mathbf{A}$

Signals are letters followed by the independent variable between parentheses for continuous signals and brackets for discrete signals. For frequency-domain signals the letter is uppercase.

Matrix operations we use the apex ^{T} to indicate matrix transposition and the dagger † for the Hermitian transpose ($^\dagger = ^{T*}$)

Discrete Fourier Transform is always normalized. The N_f-point DFT is defined as

$$X[k] = \sqrt{\frac{1}{N_\mathrm{f}}} \sum_{n=0}^{N_\mathrm{f}-1} x[n] e^{-j2\pi \frac{nk}{N_\mathrm{f}}}$$

while the IDFT is

$$x[n] = \sqrt{\frac{1}{N_\mathrm{f}}} \sum_{n=0}^{N_\mathrm{f}-1} X[k] e^{+j2\pi \frac{nk}{N_\mathrm{f}}}$$

Autocorrelation of sequences are defined as

$$\psi_x[k] = \sum_{n=-\infty}^{+\infty} x^*[n] x[n+k]$$

for finite energy sequences and

$$\psi_x[k] = \mathbb{E}\left\{x^*[n]x[n+k]\right\}$$

for finite power sequences

Power Spectral Densities of sequences are indicated with the letter Ψ and are defined as the Discrete-Time Fourier Transform of the autocorrelation function $\psi[k]$

$$\Psi_x\left(e^{j2\pi fT}\right) = \sum_{k=-\infty}^{+\infty} \psi_x[k]e^{-j2\pi fkT}$$

for finite power sequences

A.2 Complex baseband

A signal transmitted over optical fiber is a *passband* signal around the carrier frequency f_0, *i.e.* its power spectral density $\Psi_{x,\mathrm{pb}}(f)$ is nonzero only in a frequency range around f_0

$$\Psi_{x,\mathrm{pb}}(f) \neq 0 \qquad \forall f \,:\, 0 < f_0 - \frac{B}{2} \leq |f| \leq f_0 + \frac{B}{2} < \infty$$

Real world signals are real, so they have Hermitian symmetry in frequency domain

$$x_{\mathrm{pb}}(t) \in \Re \quad \Longleftrightarrow \quad X_{\mathrm{pb}}(f) = X^*_{\mathrm{pb}}(-f) \tag{A.1}$$

and the quantity B is called *bandwidth* of the signal, which for real signals it is calculated only for positive frequencies

Pass-band signals are painful to handle, so we can use these two properties to find an alternative representation. This leads to the *upconversion theorem* which states that every passband signal can be written as a function of two real *baseband* signals $x_{\mathrm{I}}(t)$ and $x_{\mathrm{Q}}(t)$, *i.e.* their power spectral density is nonzero in a range of frequencies around the DC $f = 0$

$$\Psi_{x_{\mathrm{I}}}(f), \Psi_{x_{\mathrm{Q}}}(f) \neq 0 \qquad \forall f \,:\, |f| \leq \frac{B}{2} < \infty$$

each with bandwidth $B/2$.

The upconversion theorem [4, 29] states that

$$x_{\mathrm{pb}}(t) = \sqrt{2}x_{\mathrm{I}}(t)\cos\left(2\pi f_0 t\right) - \sqrt{2}x_{\mathrm{Q}}(t)\sin\left(2\pi f_0 t\right) = \sqrt{2}\Re\Big\{\underbrace{\left[x_{\mathrm{I}}(t) + jx_{\mathrm{Q}}(t)\right]}_{x(t)} e^{j2\pi f_0 t}\Big\} =$$

$$= \sqrt{2}\Re\left\{x(t)e^{j2\pi f_0 t}\right\}$$

where we collected the two real baseband signals in a complex baseband signal

$$x(t) = x_{\mathrm{I}}(t) + jx_{\mathrm{Q}}(t) = e(t)e^{j\theta(t)}$$

called *complex baseband* of $x_{\mathrm{pb}}(t)$. In details, $x_{\mathrm{I}}(t)$ and $x_{\mathrm{Q}}(t)$ are called In-Phase (I) and Quadrature (Q) components of $x(t)$, and $e(t)$ and $\theta(t)$ *envelope* and *phase* of $x(t)$. Since $x(t)$ is a complex signal, the bandwidth is B since we are taking into account also the negative frequencies.

To transform a passband signal into its complex baseband representation we perform the *complex downconversion* process

$$x(t) = \frac{\sqrt{2}}{2} \left[x_{\mathrm{pb}}(t) + j\, \mathcal{H} \left\{ x_{\mathrm{pb}}(t) \right\} \right] e^{-j2\pi f_0 t}$$

where $\mathcal{H}$ indicates Hilbert transform, defined in (2.7).

Since there's a $1:1$ correspondence between a passband signal and its complex envelope, unless explicitly written, *all* the signals in this work are expressed in the complex baseband notation.

Bibliography

[1] Govind P. Agrawal. *Fiber-Optic Communication System*. Fourth Edition. Wiley, 2010.

[2] Rod C Alferness. "Waveguide electrooptic modulators." In: *IEEE Transactions on Microwave Theory Techniques* 30 (1982), pp. 1121–1137.

[3] Daniel JF Barros and Joseph M Kahn. "Comparison of orthogonal frequency-division multiplexing and on-off keying in amplified direct-detection single-mode fiber systems." In: *Journal of Lightwave Technology* 28.12 (2010), pp. 1811–1820.

[4] John R Barry, Edward A Lee, and David G Messerschmitt. *Digital communication*. Third Edition. Springer, 2004.

[5] Jorge Campello. "Practical bit loading for DMT." In: *Communications, 1999. ICC'99. 1999 IEEE International Conference on*. Vol. 2. IEEE. 1999, pp. 801–805.

[6] T. Chan, I-Cheng Lu, Jyehong Chen, and W.I. Way. "400-Gb/s Transmission Over 10-km SSMF Using Discrete Multitone and 1.3-µm EMLs." In: *Photonics Technology Letters, IEEE* 26.16 (Aug. 2014), pp. 1657–1660.

[7] Jacky S. Chow, Jerry C. Tu, and John M. Cioffi. "A discrete multitone transceiver system for HDSL applications." In: *Selected Areas in Communications, IEEE Journal on* 9.6 (1991), pp. 895–908.

[8] Peter S Chow, John M Cioffi, and J Bingham. "A practical discrete multitone transceiver loading algorithm for data transmission over spectrally shaped channels." In: *IEEE Transactions on communications* 43.234 (1995), pp. 773–775.

[9] John M. Cioffi. "Chapter 4–Multi-channel Modulation." In: *Lecture notes for advanced digital communications*. Stanford University, 2001.

[10] Robert FH Fischer. *Precoding and signal shaping for digital transmission*. John Wiley & Sons, 2005.

[11] Cisco Visual Networking Index. "The zettabyte era–trends and analysis." In: *Cisco white paper* (2013).

[12] ITU-T. *Asymmetric digital subscriber line (ADSL) transceivers*. Recommendation G.992.1. Geneva: International Telecommunication Union, July 1999.

[13] ITU-T. *Characteristics of a dispersion-shifted, single-mode optical fibre and cable*. Recommendation G.653. Geneva: International Telecommunication Union, July 2010.

[14] ITU-T. *Characteristics of a single-mode optical fibre and cable*. Recommendation G.652. Geneva: International Telecommunication Union, Nov. 2009.

[15] ITU-T. *Optical system design and engineering considerations*. Supplement 39. Geneva: International Telecommunication Union, Sept. 2012.

[16] Yutaka Kai, Masato Nishihara, Toshiki Tanaka, Tomoo Takahara, Lei Li, Zhenning Tao, Bo Liu, Jens C Rasmussen, and Tomislav Drenski. "Experimental comparison of pulse amplitude modulation (PAM) and discrete multi-tone (DMT) for short-reach 400-Gbps data communication." In: *Optical Communication (ECOC 2013), 39th European Conference and Exhibition on*. IET. 2013, pp. 1–3.

[17] K C Kao and George A Hockham. "Dielectric-fibre surface waveguides for optical frequencies." In: *Proceedings of the Institution of Electrical Engineers* 113.7 (1966), pp. 1151–1158.

[18] Jeffrey Lee, Florian Breyer, Sebastian Randel, Olaf Ziemann, Henrie P van den Boom, and Antonius M Koonen. "Low-cost and robust 1-Gbit/s plastic optical fiber link based on light-emitting diode technology." In: *Optical Fiber Communication Conference*. Optical Society of America. 2008, OWB3.

[19] SC Lee, Florian Breyer, Sebastian Randel, Roberto Gaudino, Gabriella Bosco, Andreas Bluschke, Michael Matthews, Philipp Rietzsch, Rainer Steglich, Henrie van den Boom, et al. "Discrete multitone modulation for maximizing transmission rate in step-index plastic optical fibers." In: *Journal of Lightwave Technology* 27.11 (2009), pp. 1503–1513.

[20] Howard E Levin. "A complete and optimal data allocation method for practical discrete multitone systems." In: *Global Telecommunications Conference, 2001. GLOBECOM'01. IEEE*. Vol. 1. IEEE. 2001, pp. 369–374.

[21] Paul Little. *Who's afraid of the Big, Bad DSP?* Tech. rep. Fujitsu Semiconductor America, Inc., July 2014. URL: http://goo.gl/tKC2op.

[22] Theodore H Maiman. "Stimulated Optical Radiation in Ruby." In: *Nature* 4736 (1960), pp. 493–494.

[23] DG Mestdagh, Paul Spruyt, and Bernard Biran. "Analysis of clipping effect in DMT-based ADSL systems." In: *Communications, 1994. ICC'94, SUPERCOMM/ICC'94, Conference Record,'Serving Humanity Through Communications.'IEEE International Conference on*. IEEE. 1994, pp. 293–300.

[24] Terenuma Miya, Y Terunuma, T Hosaka, and To Miyashita. "Ultimate low-loss single-mode fibre at 1.55 µm." In: *Electronics Letters* 15.4 (1979), pp. 106–108.

[25] Laia Nadal, Michela Svaluto Moreolo, Josep M Fàbrega, Annika Dochhan, Helmut Grießer, Michael Eiselt, and Jörg-Peter Elbers. "DMT Modulation With Adaptive Loading for High Bit Rate Transmission Over Directly Detected Optical Channels." In: *Journal of Lightwave Technology* 32.21 (2014), pp. 3541–3551.

[26] Harry Nyquist. "Certain topics in telegraph transmission theory." In: *American Institute of Electrical Engineers, Transactions of the* 47.2 (1928), pp. 617–644.

[27] Annachiara Pagano, Emilio Riccardi, Marco Bertolini, Vitaliano Farelli, and Tony Van De Velde. "400Gb/s Real-time Trial Using Rate-adaptive Transponders for Next Generation Flexible-grid Networks." In: *Optical Fiber Communication Conference*. Optical Society of America. 2014, Tu2B–4.

[28] Wei-Ren Peng, Bo Zhang, Kai-Ming Feng, Xiaoxia Wu, Alan E Willner, and Sien Chi. "Spectrally efficient direct-detected OFDM transmission incorporating a tunable frequency gap and an iterative detection techniques." In: *Lightwave Technology, Journal of* 27.24 (2009), pp. 5723–5735.

[29] John Proakis and Masoud Salehi. *Digital communications*. Fifth Edition. McGraw-Hill, 2007.

[30] Sebastian Randel, Florian Breyer, Sian CJ Lee, and Joachim W Walewski. "Advanced modulation schemes for short-range optical communications." In: *Selected Topics in Quantum Electronics, IEEE Journal of* 16.5 (2010), pp. 1280–1289.

[31] Sebastian Randel, Dario Pilori, S. Chandrasekhar, Greg Raybon, and Peter Winzer. "100-Gb/s Discrete-Multitone Transmission Over 80-km SSMF Using Single-Sideband Modulation With Novel Interference-Cancellation Scheme." In: *Optical Communication (ECOC), 2015 European Conference on*. IEEE. 2015, pp. 1–3.

[32] Sebastian Randel, Dario Pilori, Stephen Corteselli, Gregory Raybon, Andrew Adamiecki, Alan Gnauck, S Chandrasekhar, Peter J Winzer, Lars Altenhain, Anna Bielik, et al. "All-Electronic Flexibly Programmable 864-Gb/s Single-Carrier PDM-64-QAM." In: *Optical Fiber Communication Conference*. Optical Society of America. 2014, Th5C–8.

[33] Sebastian Randel, Stephen Corteselli, Peter J Winzer, Andrew Adamiecki, Alan Gnauck, S Chandrasekhar, Anna Bielik, Lars Altenhain, Tobias Ellermeyer, Ulrich Dümler, et al. "Generation of a Digitally Shaped 55-GBd 64-QAM Single-Carrier Signal Using Novel High-Speed DACs." In: *Optical Fiber Communication Conference*. Optical Society of America. 2014, M2A–3.

[34] J.C. Rasmussen, T. Takahara, T. Tanaka, Y. Kai, M. Nishihara, T. Drenski, Lei Li, Weizhen Yan, and Zhenning Tao. "Digital signal processing for short reach optical links." In: *Optical Communication (ECOC), 2014 European Conference on*. Sept. 2014, pp. 1–3.

[35] Seb J Savory, Giancarlo Gavioli, Robert I Killey, and Polina Bayvel. "Electronic compensation of chromatic dispersion using a digital coherent receiver." In: *Optics Express* 15.5 (2007), pp. 2120–2126.

[36] C.E. Shannon. “A mathematical theory of communication.” In: *Bell System Technical Journal, The* 27.4 (Oct. 1948), pp. 623–656.

[37] Toshiki Tanaka, Tomoo Takahara, and Jens C Rasmussen. *Discrete Multi-tone Technology for 100G Ethernet*. Tech. rep. Fujitsu Laboratories Ltd., Sept. 2012.

[38] Jan-Jaap Van de Beek, Magnus Sandell, Per Ola Borjesson, et al. “ML estimation of time and frequency offset in OFDM systems.” In: *IEEE transactions on signal processing* 45.7 (1997), pp. 1800–1805.

[39] Peter Winzer. “Beyond 100G ethernet.” In: *Communications Magazine, IEEE* 48.7 (2010), pp. 26–30.

[40] PJ Winzer, G Raybon, and Marcus Duelk. “107-Gb/s optical ETDM transmitter for 100G Ethernet transport.” In: *Optical Communication, 2005. ECOC 2005. 31st European Conference on*. Vol. 6. IET. 2005, pp. 1–2.

[41] Tiejun J. Xia and Glenn A. Wellbrock. “Chapter 2 - Commercial 100-Gbit/s Coherent Transmission Systems.” In: *Optical Fiber Telecommunications*. Ed. by Ivan P. Kaminow, Tingye Li, and Alan E. Willner. Sixth Edition. Optics and Photonics. Boston: Academic Press, 2013, pp. 45–82.

[42] Chongjin Xie, Po Dong, Sebastian Randel, Dario Pilori, Peter J. Winzer, Silvia Spiga, Benjamin Kögel, Christian Neumeyr, and Markus Amann. “Single-VCSEL 100-Gb/s Short-Reach System Using Discrete Multi-Tone Modulation and Direct Detection.” In: *Optical Fiber Communication Conference*. Optical Society of America, 2015, Tu2H.2.

[43] Weizhen Yan, Lei Li, Bo Liu, Hao Chen, Zhenning Tao, Toshiki Tanaka, Tomoo Takahara, Jens Rasmussen, and Drenski Tomislav. “80 km IM-DD Transmission for 100 Gb/s per Lane Enabled by DMT and Nonlinearity Management.” In: *Optical Fiber Communication Conference*. Optical Society of America. 2014, pp. M2I–4.

[44] Kazushige Yonenaga and Noboru Takachio. “A fiber chromatic dispersion compensation technique with an optical SSB transmission in optical homodyne detection systems.” In: *Photonics Technology Letters, IEEE* 5.8 (1993), pp. 949–951.

[45] Qiang Zhang, Yuanyuan Fang, Enbo Zhou, Tianjian Zuo, Liang Zhang, Gordon Ning Liu, and Xiaogeng Xu. “C-band 56Gbps transmission over 80-km single mode fiber without chromatic dispersion compensation by using intensity-modulation direct-detection.” In: *Optical Communication (ECOC), 2014 European Conference on*. IEEE. 2014, pp. 1–3.